2016-09

Extending the calibration in the Underwater Sound Reference Division (USRD) reciprocity coupler to incorporate phase

Slater, William H.

Monterey, California: Naval Postgraduate School

NAVAL POSTGRADUATE SCHOOL

MONTEREY, CALIFORNIA

THESIS

EXTENDING THE CALIBRATION IN THE UNDERWATER SOUND REFERENCE DIVISION (USRD) RECIPROCITY COUPLER TO INCORPORATE PHASE

by

William H. Slater

September 2016

Thesis Co-Advisors: Steven R. Baker
Steven E. Crocker
Daphne Kapolka

THIS PAGE INTENTIONALLY LEFT BLANK

REPORT DOCUMENTATION PAGE

Form Approved OMB No. 0704–0188

1. AGENCY USE ONLY *(Leave Blank)*	2. REPORT DATE	3. REPORT TYPE AND DATES COVERED
	September 2016	Master's Thesis 08-01-2014 to 08-21-2016

4. TITLE AND SUBTITLE

EXTENDING THE CALIBRATION IN THE UNDERWATER SOUND REFERENCE DIVISION (USRD) RECIPROCITY COUPLER TO INCORPORATE PHASE

5. FUNDING NUMBERS

6. AUTHOR(S)

William H. Slater

7. PERFORMING ORGANIZATION NAME(S) AND ADDRESS(ES)

Naval Postgraduate School
Monterey, CA 93943

8. PERFORMING ORGANIZATION REPORT NUMBER

9. SPONSORING / MONITORING AGENCY NAME(S) AND ADDRESS(ES)

N/A

10. SPONSORING / MONITORING AGENCY REPORT NUMBER

11. SUPPLEMENTARY NOTES

The views expressed in this document are those of the author and do not reflect the official policy or position of the Department of Defense or the U.S. Government. IRB Protocol Number: N/A.

12a. DISTRIBUTION / AVAILABILITY STATEMENT

Approved for public release. Distribution is unlimited.

12b. DISTRIBUTION CODE

13. ABSTRACT *(maximum 200 words)*

In this report, a phase measurement is added to the Underwater Sound Reference Division (USRD) reciprocity coupler primary calibration procedure for an H48 reference hydrophone. Data acquisition equipment is added to record time-series data from the hydrophone under test and from the reciprocal transducers. The complex-valued hydrophone sensitivity is calculated. The sensitivity magnitude is compared to measurements from the standard coupler calibration procedure, and the complex sensitivity data are also fitted to a simple high-pass circuit model. The model is used to estimate the low-frequency cutoff of H48 hydrophone SN4. The low-frequency cutoff measured in this report is about 0.2 Hz higher than that originally measured and specified when the H48 hydrophones were first built. The new results show significant roll-off in phase below 10-20 Hz, a range where the phase is typically assumed flat during the standard calibration. By 1 Hz the phase roll-off is about 20°. The error analysis of the original coupler is summarized and error and uncertainty due to new data acquisition equipment and phase measurement added. Some errors due to simplifications in the acoustics of the coupler are left to future work.

14. SUBJECT TERMS

acoustic, calibration, coupler, reciprocity, phase, uncertainty, complex uncertainty, H48, hydrophone, Underwater Sound Reference Division, USRD

15. NUMBER OF PAGES 71

16. PRICE CODE

17. SECURITY CLASSIFICATION OF REPORT	18. SECURITY CLASSIFICATION OF THIS PAGE	19. SECURITY CLASSIFICATION OF ABSTRACT	20. LIMITATION OF ABSTRACT
Unclassified	Unclassified	Unclassified	UU

NSN 7540-01-280-5500

Standard Form 298 (Rev. 2–89)
Prescribed by ANSI Std. 239–18

THIS PAGE INTENTIONALLY LEFT BLANK

Approved for public release. Distribution is unlimited.

EXTENDING THE CALIBRATION IN THE UNDERWATER SOUND REFERENCE DIVISION (USRD) RECIPROCITY COUPLER TO INCORPORATE PHASE

William H. Slater
Civilian, Department of the Navy
B.S., Washington University in St. Louis, 2009

Submitted in partial fulfillment of the
requirements for the degree of

MASTER OF SCIENCE IN ENGINEERING ACOUSTICS

from the

NAVAL POSTGRADUATE SCHOOL
September 2016

Approved by: Steven R. Baker
Thesis Co-Advisor

Steven E. Crocker
Thesis Co-Advisor

Daphne Kapolka
Thesis Co-Advisor and Chair
Engineering Acoustics Academic Committee

THIS PAGE INTENTIONALLY LEFT BLANK

ABSTRACT

In this report, a phase measurement is added to the Underwater Sound Reference Division (USRD) reciprocity coupler primary calibration procedure for an H48 reference hydrophone. Data acquisition equipment is added to record time-series data from the hydrophone under test and from the reciprocal transducers. The complex-valued hydrophone sensitivity is calculated. The sensitivity magnitude is compared to measurements from the standard coupler calibration procedure, and the complex sensitivity data are also fitted to a simple high-pass circuit model. The model is used to estimate the low-frequency cutoff of H48 hydrophone SN4. The low-frequency cutoff measured in this report is about 0.2 Hz higher than that originally measured and specified when the H48 hydrophones were first built. The new results show significant roll-off in phase below 10-20 Hz, a range where the phase is typically assumed flat during the standard calibration. By 1 Hz the phase roll-off is about 20°. The error analysis of the original coupler is summarized and error and uncertainty due to new data acquisition equipment and phase measurement added. Some errors due to simplifications in the acoustics of the coupler are left to future work.

THIS PAGE INTENTIONALLY LEFT BLANK

Table of Contents

THIS PAGE INTENTIONALLY LEFT BLANK

List of Figures

List of Tables

THIS PAGE INTENTIONALLY LEFT BLANK

List of Acronyms and Abbreviations

DC	direct current
DOD	Department of Defense
FFVS	free-field voltage sensitivity
NIST	National Institute of Standards and Technology
NPS	Naval Postgraduate School
ONI	Office of Naval Intelligence
RC	resistor-capacitor
USN	U.S. Navy
USRD	Underwater Sound Reference Division

THIS PAGE INTENTIONALLY LEFT BLANK

Acknowledgments

I would like to thank my advisers Professor Baker, Dr. Crocker, and Professor Kapolka for their interest in my topic and technical guidance. I would like to thank Greg Blasdell for taking time to show me how to run the USRD coupler and for his thorough test setups and troubleshooting that made my job much easier. I would like to thank Bob Drake for helping me to understand Joseph Zalesak's notes and papers. And I'd like to thank Scott Greenberg, for his patient support and confidence that I would eventually finish this thesis.

THIS PAGE INTENTIONALLY LEFT BLANK

CHAPTER 1:
Introduction

The Underwater Sound Reference Division (USRD) reciprocity coupler is used to calibrate the reference hydrophones that disseminate the primary calibration to the secondary references used by the U.S. Navy (USN) and other organizations.

To completely reproduce an acoustic waveform during calibration, the magnitude and phase of the waveform are required. Historically, hydrophone calibration is more often performed gathering only magnitude information from the hydrophone under test. Phase response is more difficult to measure accurately and can be assumed constant when hydrophones are operating well below their resonance frequencies and above their low-frequency cutoff. The current USRD coupler calibration procedure for the H48 reference hydrophone measures magnitude only and assumes a constant phase response over the bandwidth from 5 Hz-2000 Hz. The reference hydrophones are operating well below their first resonance, but the bottom of the frequency range can be affected by the hydrophone's low-frequency cutoff, especially for tests where secondary references are used to measure frequencies below 5 Hz. Adding a phase measurement to the calibration would reduce the phase error at the low end of the calibration frequency range where the phase response is no longer constant. These phase errors can undermine accurate direction finding and degrade broadband measurements made by sonar arrays.

As demand rises for phase measurements, an accurate phase calibration of USRD primary references becomes more important. The USN can use this information to enhance accuracy in beamforming, in broadband applications, and in low-frequency sound pressure measurements required by the Office of Naval Intelligence (ONI). Modern towed arrays could be supplied with more accurate calibrations at the low end of their operating frequency band. Phase information will allow for measurement of the resistor-capacitor (RC) time constant of the equivalent single-pole high-pass filter circuit at the input to the preamplifier in a hydrophone channel of a towed array, an important quality control parameter. An out-of-specification RC time constant can lead to phase response errors between otherwise identical hydrophones. This constant increases as parasitic resistances in the hydrophone

increase and as the input resistance to the preamplifier decreases. An RC time constant that increases over the time can render an array unable to accurately measure signals it was previously calibrated to measure. Phase calibration of hydrophones will complement the magnitude calibration and allow the RC time constant to be measured and tracked without taking the array apart.

Hydrophone phase calibrations can be performed in a variety of ways. Luker and Van Buren [1] performed a phase calibration in an open tank using a three-transducer reciprocity method. The projector, hydrophone, and reciprocal transducer were all arranged in a straight line, with the hydrophone in the center. The hydrophone could be rotated in place to face either the projector or reciprocal transducer or be removed from the tank, eliminating phase errors due to distance between the transducers and hydrophone, and sound speed. Hayman et al. [2] performed a free-field reciprocity calibration, with phase, in an open tank facility, then compared the results to a phase calibration using optical interferometry. In that setup, a thin, acoustically transparent, optically reflective membrane called a pellicle is placed a fixed distance from a source and an optical interferometer or laser vibrometer is used to measure acoustic particle velocity at the pellicle. The pellicle is then replaced with the hydrophone under test, and hydrophone voltage measurements taken with the same source are used with the acoustic pressure to calculate sensitivity. The location of the acoustic center of the hydrophone must be carefully matched to the location of the pellicle.

The USRD reciprocity coupler provides an accurate and consistent primary calibration up to very high pressure that is not subject to many of the sources of error in the above mentioned methods, due to the equipment setup and the physics of the coupler procedure. This paper explains how a phase measurement was added to the USRD reciprocity coupler. In short, the magnitude and phase of all electrical parameters in the reciprocity calibration procedure must be measured and the complex-valued reciprocity parameter must be used.

CHAPTER 2:
Theory

The reciprocity coupler is a fluid-filled cavity in which three transducers are installed to perform a reciprocity calibration to calculate the low-frequency, free-field sensitivity of an unknown hydrophone. Figure 2.1 shows the cross section of an example coupler. Identical transducers are installed on the left and right sides of the coupler and a reference hydrophone (to be calibrated) in the center. Castor oil fills the sealed cavity.

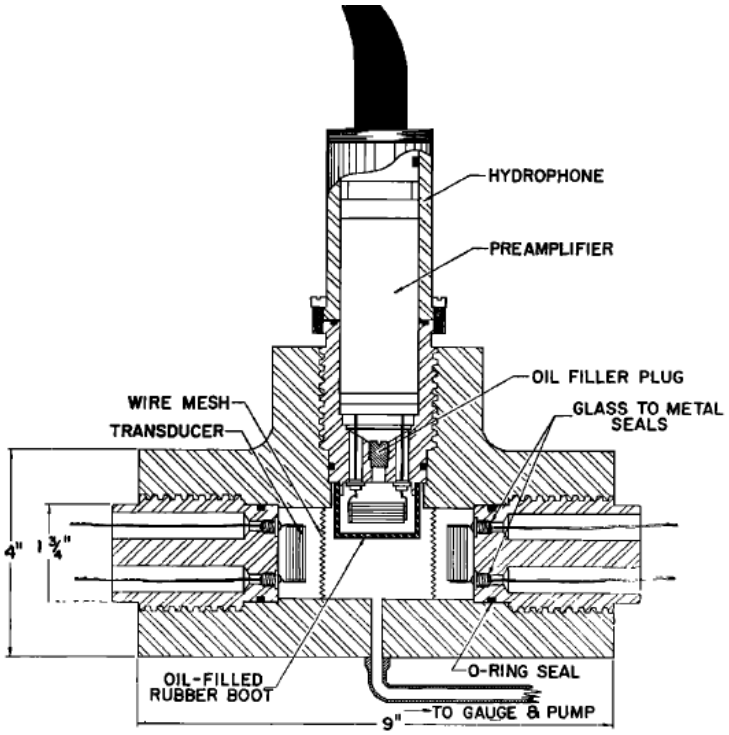

Figure 2.1. A cross-section view of three transducers installed in an example reciprocity coupler. Source: [3].

The pressure sensitivity is obtained via the reciprocity method by measuring the current to the projector and the voltages at the receiving transducer and unknown hydrophone. The reciprocity parameter ties these measurements to the sensitivity of the unknown hydrophone. The coupler is designed around a set of assumptions that, when satisfied, ensure the pres-

sure and free-field sensitivities are equal, allowing the more useful free-field sensitivity measurement to be calculated during the calibration.

Throughout this report, complex quantities are shown in bold font.

2.1 Coupler Calibration Assumptions

Several assumptions are made when performing a calibration in a reciprocity coupler to enforce the condition that the sound pressure is the same everywhere in the coupler at a given instant in time, as described in [4]:

1. The wavelength of sound must be much larger than the largest dimension of coupler, its length.
2. The walls of the coupler and transducer elements must be rigid — they must have a much higher impedance than the acoustic medium.
3. No air or any other low impedance material can be present in the coupler.

The hydrophone sensitivity measured in the coupler is the pressure sensitivity, but the free-field sensitivity is the desired measurement. Fortunately, in the conditions of the coupler, the pressure sensitivity and free-field sensitivity are equivalent. Figure 2.2 shows a hydrophone with an open circuit voltage, $\boldsymbol{e}$, and an acoustical impedance, $\boldsymbol{Z_a}$. The applied pressure at the acoustic input in the coupler is $\boldsymbol{p_a}$ and an acoustical Thevenin generator represents the effects of a free field: the radiation impedance, $\boldsymbol{Z_r}$, and the blocked and free-field pressures, $\boldsymbol{p_b}$ and $\boldsymbol{p_f}$. The ratio $\frac{p_b}{p_f}$ is called the diffraction constant, $\boldsymbol{D}$, although it varies with frequency.

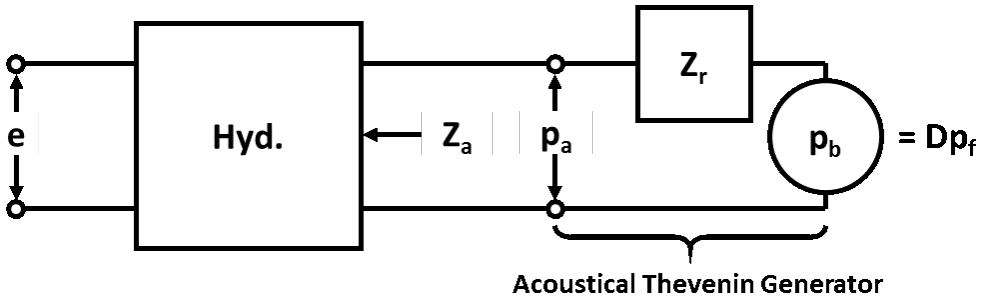

Figure 2.2. An equivalent circuit of a hydrophone in a free field. Source: [4].

In order for p_f and p_b to be equal, the diffraction constant D must be equal to 1, a condition satisfied if the hydrophone is much smaller than an acoustic wavelength, which must be true if the wavelength of the sound is much larger than the coupler cavity. Analyzing the circuit diagram, p_b and p_a can be considered equal if Z_r is much smaller than Z_a. In situations where the hydrophone's physical dimensions are much smaller than the wavelengths, Z_r will be small and the $Z_r << Z_a$ criteria will be met by a piezoelectric transducer operated at frequencies away from resonance. With these two criteria met, the free-field pressure is equivalent to the applied pressure at the acoustic input [4].

2.2 Reciprocity Calculation for the Complex Voltage Sensitivity

The primary calibration performed using the USRD reciprocity coupler takes advantage of the reciprocity method to calculate the complex voltage sensitivity of an unknown hydrophone. In a reciprocity calibration, the voltage sensitivity of a hydrophone can be calculated through the measurement of six electrical parameters made on three transducers (reciprocal transducers X and Y, and a hydrophone) as shown in Table 2.1. Two measurement setups are required to obtain all six electrical parameters, (a) reciprocal transducer X transmitting and reciprocal transducer Y and hydrophone receiving, and (b) reciprocal transducer Y transmitting and reciprocal transducer X and hydrophone receiving. The electrical parameters are: i_X, the input current to transducer X when it is transmitting, e_{HX}, the open-circuit output voltage from the hydrophone when transducer X is transmitting, e_{YX}, the open-circuit output voltage from transducer Y when transducer X is transmitting, i_Y, the input current to transducer Y when it is transmitting, e_{HY}, the open-circuit output voltage from the hydrophone when transducer Y is transmitting, and e_{XY}, the open-circuit output voltage from transducer X when transducer Y is transmitting.

The output voltage measurements can be expressed in terms of a voltage sensitivity and the pressure transmitted by the transmitting transducer. They are manipulated with the goal of expressing the sensitivity of the unknown hydrophone while eliminating any acoustical parameters of the other transducers in order to produce a primary calibration as shown in [4]. For configuration (a) this expression is

$$e_{HX} = M_H p_X = M_H i_X S_X \,, \tag{2.1}$$

Table 2.1. Reciprocity calibration measurement groupings. Adapted from [4].

Configuration	Input Current Measurement	Transmitting Transducer	Receiving Transducers	Output Voltage Measurements
(a)	$\boldsymbol{i_X}$	Reciprocal Transducer X	Hydrophone, Reciprocal Transducer Y	$\boldsymbol{e_{HX}}$, $\boldsymbol{e_{YX}}$
(b)	$\boldsymbol{i_Y}$	Reciprocal Transducer Y	Hydrophone, Reciprocal Transducer X	$\boldsymbol{e_{HY}}$, $\boldsymbol{e_{XY}}$

where $\boldsymbol{M_H}$ is the open-circuit receiving voltage sensitivity of the hydrophone and $\boldsymbol{S_X}$ is the transmitting current response of reciprocal transducer X. Unlike the free-field form of this expression, there is no dependence on separation distances, and the transmitting current response is the pressure inside the cavity for a given current — there is no reference distance term. Similarly, the open-circuit output voltage of the transducer Y is

$$\boldsymbol{e_{YX}} = \boldsymbol{M_Y i_X S_X}\,, \tag{2.2}$$

where $\boldsymbol{M_Y}$ is the open-circuit receiving voltage sensitivity of reciprocal transducer Y. The ratio of the output voltages in configuration (a) is

$$\frac{\boldsymbol{e_{HX}}}{\boldsymbol{e_{YX}}} = \frac{\boldsymbol{M_H}}{\boldsymbol{M_Y}}. \tag{2.3}$$

From configuration (b)

$$\boldsymbol{e_{HY}} = \boldsymbol{M_H i_Y S_Y}\,, \tag{2.4}$$

where $\boldsymbol{S_Y}$ is the transmitting current response of reciprocal transducer Y. Using the property of the reciprocal transducer that the ratio of the receiving sensitivity and transmitting response is equal to the reciprocity parameter,

$$\boldsymbol{J} = \frac{\boldsymbol{M_Y}}{\boldsymbol{S_Y}}\,, \tag{2.5}$$

which is only a function of acoustical properties of the coupler fluid medium. Equations

2.3, 2.4, and 2.5 can be solved for the hydrophone sensitivity as shown in Equation 2.6.

$$\boldsymbol{M_H} = \sqrt{\frac{\boldsymbol{e_{HY}e_{HX}}}{\boldsymbol{e_{YX}i_Y}}\boldsymbol{J}}. \tag{2.6}$$

In the USRD coupler calibration procedure, redundant measurements using reciprocal transducers X and Y as both a projector and receiver reduce measurement uncertainty and create convenient symmetry to simplify phase measurement. Measurement (b) in Table 2.1 is collected when the cables driving the projecting transducer and recording from the receiving transducer are interchanged from configuration (a), and the measurement is repeated. The extra output voltage measurement, $\boldsymbol{e_{XY}}$, is incorporated into the denominator of Equation 2.6 where the geometric mean of both receiving transducer measurements gives

$$\boldsymbol{M_H} = \sqrt{\frac{\boldsymbol{e_{HX}e_{HY}}}{\sqrt{\boldsymbol{e_{YX}i_X} \times \boldsymbol{e_{XY}i_Y}}}\boldsymbol{J}}. \tag{2.7}$$

In this coupler setup, current measurements are obtained by measuring the voltage across a standard capacitor placed in series with the input current. Using the relationships $\boldsymbol{i_X} = \boldsymbol{e_{CX}}j\omega C_p$ and $\boldsymbol{i_Y} = \boldsymbol{e_{CY}}j\omega C_p$, where $\boldsymbol{e_{CX}}$ and $\boldsymbol{e_{CY}}$ are the voltages across the standard capacitor and C_p is the capacitance of the standard capacitor, the currents in Equation 2.7 can be substituted for voltages, producing

$$\boldsymbol{M_H} = \sqrt{\frac{\boldsymbol{e_{HX}e_{HY}}}{\sqrt{\boldsymbol{e_{YX}e_{CX}} \times \boldsymbol{e_{XY}e_{CY}}}}\frac{\boldsymbol{J}}{j\omega C_p}}. \tag{2.8}$$

2.3 Reciprocity Parameter

The complex pressure reciprocity parameter, $\boldsymbol{J}$, must be calculated for a small rigid-walled cavity in order to obtain the hydrophone sensitivity from the voltage and current measurements in Equation 2.8. The beauty of the reciprocity parameter is that it depends only on acoustic properties of the fluid medium. No electrical properties of any of the transducers have to be known, making the reciprocity method a primary calibration. To derive this parameter, the definition of the reciprocity parameter as the reciprocal of the acoustical transfer impedance [5] is used.

First, assume a simplified coupler geometry as shown in Figure 2.3. This cross section of a right cylindrical cavity of length L is capped by identical, reciprocal transducers at either end. Assume plane wave motion along the x axis with no motion in the radial or angular directions. The acoustic field can be modeled by the network diagram in Figure 2.4.

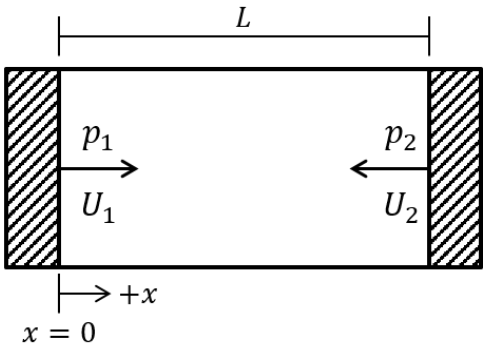

Figure 2.3. A simplified reciprocity coupler geometry consisting of a cylindrical cavity capped by two reciprocal transducers shown in cross section.

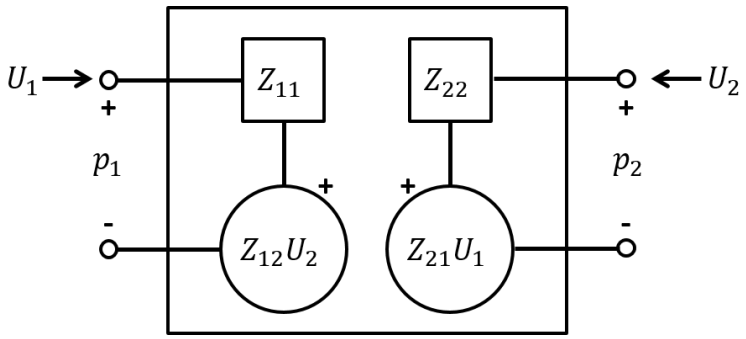

Figure 2.4. A network diagram of acoustic field inside a cylindrical cavity capped with two reciprocal transducers.

The pressure and volume velocity can be related by the mutual acoustical radiation impedance matrix in the network equations

$$\begin{pmatrix} \boldsymbol{p}_1 \\ \boldsymbol{p}_2 \end{pmatrix} = \begin{bmatrix} \boldsymbol{Z}_{11} & \boldsymbol{Z}_{12} \\ \boldsymbol{Z}_{21} & \boldsymbol{Z}_{22} \end{bmatrix} \begin{pmatrix} \boldsymbol{U}_1 \\ \boldsymbol{U}_2 \end{pmatrix}. \tag{2.9}$$

In this matrix, $\boldsymbol{Z}_{ij}$ is the ratio of the acoustic pressure at transducer i to the volume velocity of transducer j, with all other transducers but transducer j blocked. $\boldsymbol{Z}_{11}$ and $\boldsymbol{Z}_{22}$ are "self"

radiation impedances, the acoustical radiation impedance seen by one transducer when it alone is radiating; and $\boldsymbol{Z}_{12}$ and $\boldsymbol{Z}_{21}$ are "mutual" or "transfer" radiation impedances, the ratio of the blocked pressure at one transducer to the volume velocity of the other.

To derive expressions for the terms in the acoustical radiation impedance matrix, start with the relationship for the pressure of a plane wave,

$$\boldsymbol{p}(x,t) = (\boldsymbol{A}\cos(kx) + \boldsymbol{B}\sin(kx))e^{j\omega t}, \tag{2.10}$$

where $\boldsymbol{A}$ and $\boldsymbol{B}$ are constants, k is the wave number, ω is angular frequency, and t is time. From there, the particle velocity is given by

$$\boldsymbol{u}(x,t) = -\frac{1}{j\omega\rho}\frac{\partial \boldsymbol{p}}{\partial x} = \frac{k}{j\omega\rho}(\boldsymbol{A}\sin(kx) - \boldsymbol{B}\cos(kx))e^{j\omega t}. \tag{2.11}$$

The network variables $\boldsymbol{p}_1$, $\boldsymbol{p}_2$, $\boldsymbol{U}_1$, and $\boldsymbol{U}_2$ (Figure 2.4) are related to $\boldsymbol{p}(x,t)$ and $\boldsymbol{u}(x,t)$ by

$$\begin{aligned} \boldsymbol{p}_1 = \boldsymbol{p}(0,t),\ \boldsymbol{p}_2 = \boldsymbol{p}(L,t), \\ \boldsymbol{U}_1 = S\boldsymbol{u}(0,t),\ \boldsymbol{U}_2 = -S\boldsymbol{u}(L,t), \end{aligned} \tag{2.12}$$

where S is the cross sectional area of the cavity. Because the acoustical radiation impedance matrix is symmetric, only one self- and transfer impedance needs to be evaluated, and the solution can be applied to the other. Focusing on the problem where there is a transducer at $x = L$ and a rigid wall at $x = 0$, the boundary condition exists

$$\boldsymbol{U}(x=0) = 0 \therefore \boldsymbol{B} = 0. \tag{2.13}$$

Note that with $\boldsymbol{B} = 0$, the relationship in Equation 2.10 describes a standing wave.

Solving for the radiation impedance,

$$\boldsymbol{Z}_{22} = \boldsymbol{Z}_{11} = \frac{\boldsymbol{p}_2}{\boldsymbol{U}_2} = \frac{\boldsymbol{p}(L,t)}{-S\boldsymbol{u}(L,t)}\frac{\boldsymbol{A}\cos(kL)e^{j\omega t}}{\frac{-kS}{j\omega\rho}\boldsymbol{A}\sin(kL)e^{j\omega t}} = -\frac{j\rho c}{S}\cot(kL), \tag{2.14}$$

and for the acoustical transfer impedance,

$$\begin{aligned}
\boldsymbol{Z}_{12} = \boldsymbol{Z}_{21} &= \left.\frac{\boldsymbol{p}_1}{\boldsymbol{U}_2}\right|_{\boldsymbol{U}_1=0} = \frac{\boldsymbol{p}_1}{\boldsymbol{p}_2}\frac{\boldsymbol{p}_2}{\boldsymbol{U}_2} \\
&= \frac{\boldsymbol{p}_1}{\boldsymbol{p}_2}\frac{j\rho c}{S}\cot(kL) \\
&= \frac{\boldsymbol{p}(0,t)}{\boldsymbol{p}(L,t)}\frac{j\rho c}{S}\cot(kL) \\
&= \frac{\boldsymbol{A}e^{j\omega t}}{\boldsymbol{A}\cos(kL)e^{j\omega t}}\left(-\frac{j\rho c}{S}\right)\cot(kL) \\
&= -\frac{j\rho c}{S}\csc(kL).
\end{aligned}$$

Using the first two terms of a Taylor series expansion gives the following long-wavelength approximations for the self-radiation impedance

$$\boldsymbol{Z}_{22} = \boldsymbol{Z}_{11} = -\frac{j\rho c}{S}\left(\frac{1}{kL} - \frac{kL}{3}\right) = \frac{B_{ad}}{j\omega SL} + \frac{j\omega\rho L}{3} \tag{2.15}$$

and the acoustical transfer impedance

$$\boldsymbol{Z}_{12} = \boldsymbol{Z}_{21} = -\frac{j\rho c}{S}\left(\frac{1}{kL} + \frac{kL}{6}\right) = \frac{B_{ad}}{j\omega SL} - \frac{j\omega\rho L}{6}, \tag{2.16}$$

where $B_{ad} = \rho c^2$ is the adiabatic bulk modulus of the fluid. The first term in each transfer impedance shown in Equations 2.15 and 2.16 contains the bulk modulus in the numerator, a term that represents the elasticity of the coupler volume under pressure, and the frequency and volume in the denominator. This term represents the acoustical compliance of the fluid. The second term in each impedance contains the density and length in the numerator and the surface area in the denominator, forming an inertance term that describes the pressure difference required to cause a change in flow rate with time.

The reciprocity parameter, $\boldsymbol{J}$, is equal to the reciprocal of the acoustical transfer impedance [5]. Using the first term of the Taylor series expansion in powers of kL for $\boldsymbol{Z}_{12}$, from Equation 2.16, the commonly accepted reciprocity parameter for the coupler is

$$\boldsymbol{J} = \frac{1}{\boldsymbol{Z}_{12}} = \frac{j\omega SL}{\rho c^2} = j\omega C, \tag{2.17}$$

where C is the acoustical compliance of the coupler fluid medium as long as the fluid compliance is much greater than the compliance of the coupler walls and transducers. The coupler is compliance (or stiffness) dominated as long as $\frac{1}{kL} >> \frac{kL}{6}$. For the worst case conditions at the highest temperature, lowest pressure, and highest frequency in the H48 hydrophone test in this report, $\frac{1}{kL} = 1.32$ and $\frac{kL}{6} = 0.126$.

From Equation 2.8, substituting the complex pressure reciprocity calibration parameter from Equation 2.17, we get

$$\boldsymbol{M_H} = \sqrt{\frac{\boldsymbol{e_{HX}e_{HY}}}{\sqrt{\boldsymbol{e_{YX}e_{CX}} \times \boldsymbol{e_{XY}e_{CY}}}} \left(\frac{V}{C_p \rho c^2}\right)} \quad \text{V/Pa,} \tag{2.18}$$

where V is the volume of the coupler cavity. The voltage sensitivity in dB re 1Vμ/Pa is given by

$$M_H = 20 \log \left(|\boldsymbol{M_H}|\right) - 120 \quad \text{dB re 1V/}\mu\text{Pa.} \tag{2.19}$$

The factor of 120 is used to convert the dB reference to μPa. This voltage sensitivity is equivalent to the free-field voltage sensitivity while the assumptions in Section 2.1 are true.

THIS PAGE INTENTIONALLY LEFT BLANK

CHAPTER 3:
Experimental Setup and Methods

A reciprocity calibration, including phase, was performed using the USRD H48 reciprocity coupler and supporting equipment. New data acquisition equipment were used to obtain the time series data necessary to add a phase measurement. A least-squares method was used to process the time series data to obtain magnitude and phase. Systematic errors in the experimental setup were calculated and removed and a simple, equivalent-circuit high-pass filter model was fitted to the data and used to estimate the cutoff frequency of the hydrophone under test.

3.1 Physical Setup

A diagram of the physical setup is shown in Figure 3.1, with component details provided in Table 3.1 . A signal is generated at the function generator, amplified, and passed through a standard capacitor wired in series with the projector. A custom isolated differential amplifier measures the voltage across the standard capacitor, which is proportional to the current to the projector. A hand operated pressure ram controls the hydrostatic pressure in the coupler fluid, castor oil. Chamber temperature is controlled by heating or cooling distilled water from a temperature bath.

Table 3.1. Equipment List

Diagram #	Component Make/Model
1	HP 3325A
2	Krohn Hite 7500
3	Standard 1 μ F capacitor, custom differential amplifier
4	USRD H48 Reciprocity Coupler
5	Ithaco 1201
6	NI BMC-2110 and NI-6259
7	Laptop Computer with Matlab
8	Pressure Ram
9	Neslab Endocal RTE-8DD

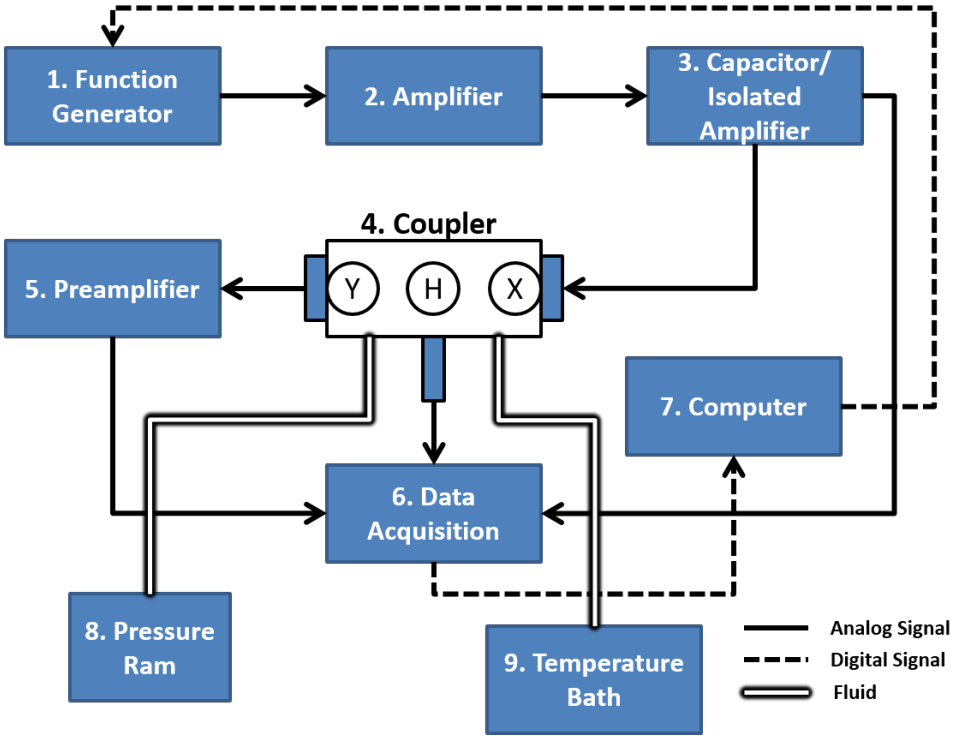

Figure 3.1. Block diagram of the experimental setup

Within the coupler, three transducers take part in the H48 USRD calibration: two reciprocal lithium sulfate spheres and the H48 reference hydrophone designed for the coupler, which also has a spherical sensing element. The reciprocal transducers are mounted on threaded steel plugs and the housing of the primary reference is designed for the threaded hole in the top of the coupler, which positions the H48's sensing element between the two reciprocal transducers. The receiving transducer is wired to a preamplifier after which the signal is recorded. The wiring to and from reciprocal transducers X and Y can be interchanged in order to record signals generated by either reciprocal transducer. The hydrophone has a built in preamplifier and is connected directly to the data acquisition equipment. A computer with Matlab is used to record the time series data and control the function generator.

3.2 Complex Signal Measurement

The magnitudes and phases of the voltages and currents required to calculate the complex sensitivity of the unknown reference hydrophone will be obtained using a least-squares

estimation process originally developed by Petr Vanicek [6]. Least-squares methods have been shown to perform better than conventional spectral analysis when the signal of interest is contaminated with systematic noise such as a direct current (DC) bias shift, a linear trend, or a sine wave of known frequency, even when that frequency is very close to that of the signal [7].

The measured voltage (or current) signals can be represented by

$$\begin{aligned} e(t_n) &= C + A\cos(2\pi f t_n + \phi) \\ &= C + A\cos(\phi)\cos(2\pi f t_n) - A\sin(\phi)\sin(2\pi f t_n), \end{aligned} \tag{3.1}$$

where $e(t_n)$ is the measured signal at any discrete time instant, t_n, A is the amplitude of the signal, ϕ is the phase of the signal, and C is a DC offset. As shown in [8], in the least-squares estimation, the design matrix is built from the equation

$$e(t_n) = \beta_0 + \beta_1\cos(2\pi f t_n) + \beta_2 sin(2\pi f t_n), \tag{3.2}$$

where the beta coefficients calculated by the least-squares fit can be used to calculate the DC offset, signal amplitude, and signal phase by comparison with Equation 3.1.

The beta coefficients can be used to reconstruct a complex signal, e, given by

$$e = Ae^{j\phi}, \tag{3.3}$$

where

$$A = \sqrt{\beta_1^2 + \beta_2^2} \tag{3.4}$$

and

$$\phi = \tan^{-1}\left(\frac{-\beta_2}{\beta_1}\right). \tag{3.5}$$

The complex signal representation

$$e = \beta_1 + j\beta_2 \tag{3.6}$$

is used to calculate hydrophone sensitivity rather than magnitude and phase separately because it allows for more convenient processing and is necessary for proper accounting of

measurement uncertainty, discussed later.

This model is used in the typical least squares form

$$y = X\beta, \tag{3.7}$$

where

$$y = \begin{bmatrix} e(t_0) \\ e(t_1) \\ \vdots \\ e(t_n) \end{bmatrix}, \quad X = \begin{bmatrix} 1 & \cos(2\pi f t_0) & \sin(2\pi f t_0) \\ 1 & \cos(2\pi f t_1) & \sin(2\pi f t_1) \\ \vdots & \vdots & \vdots \\ 1 & \cos(2\pi f t_n) & \sin(2\pi f t_n) \end{bmatrix}, \quad \text{and} \quad \beta = \begin{bmatrix} \beta_0 \\ \beta_1 \\ \beta_2 \end{bmatrix}. \tag{3.8}$$

The vector of coefficients β can be solved for given a vector of values y with a matrix of values X as

$$\beta = (X^T X)^{-1} X^T y. \tag{3.9}$$

3.3 Systematic Errors and Corrections

The systematic errors in the coupler measurement apparatus contribute more to the total error than the uncertainties in the measurements and their relevant constants. These (systematic) errors arise from simplifying theoretical assumptions not fully borne out in the measurement setup and phase error introduced from the phase responses of the measurement equipment.

Systematic phase corrections are applied to 2.18 as given by

$$\boldsymbol{M_H^{PhCor}} = \sqrt{\frac{\boldsymbol{e_{HX}}\boldsymbol{e_{HY}}}{\sqrt{(\boldsymbol{G}_{2-3a}\boldsymbol{e_{YX}})(\boldsymbol{G}_{2-3b}\boldsymbol{e_{CX}}) \times (\boldsymbol{G}_{2-3a}\boldsymbol{e_{XY}})(\boldsymbol{G}_{2-3b}\boldsymbol{e_{CY}})}} \left(\frac{V}{C_p \rho c^2}\right)} \quad \text{V/Pa}\,, \tag{3.10}$$

where the phase shifts associated with complex gains $\boldsymbol{G}_{2-3a}$ and $\boldsymbol{G}_{2-3b}$ are defined in Section 3.3.1. The magnitude of each of these complex gains is unity.

Systematic magnitude errors are treated by Zalesak [9] and summarized in Sections 3.3.2 and 3.3.3. Those corrections are applied after the phase corrections in Equation 3.10

producing

$$\left|\boldsymbol{M}_{\boldsymbol{H}}^{PhCor}\right|^{MagCor} = \frac{F_{\mathrm{A}}F_{2\mathrm{H}}}{\sqrt{F_{2\mathrm{T}}}}\left|\boldsymbol{M}_{\boldsymbol{H}}^{PhCor}\right|. \tag{3.11}$$

F_{A} is applied to the compliance term $V/\rho c^2$ and is derived in Section 3.3.2; $F_{2\mathrm{H}}$ is applied once to e_{HX} and once to e_{HY} and is derived in 3.3.3; and $F_{2\mathrm{T}}$ is applied once to e_{YX} and once to e_{XY} and is also derived in 3.3.3.

3.3.1 Phase corrections

To isolate the phase response of the hydrophone, phase change contributions by the other components must be measured and eliminated. The block diagram in Figure 3.2 illustrates the coupler setup, which can be considered a linear electro-acoustic system. Significant measurement node locations are shown as red dots and the signal path as solid black lines. Dashed lines indicate the different measurement pathways through the system. Each component in the diagram has an associated linear complex gain element.

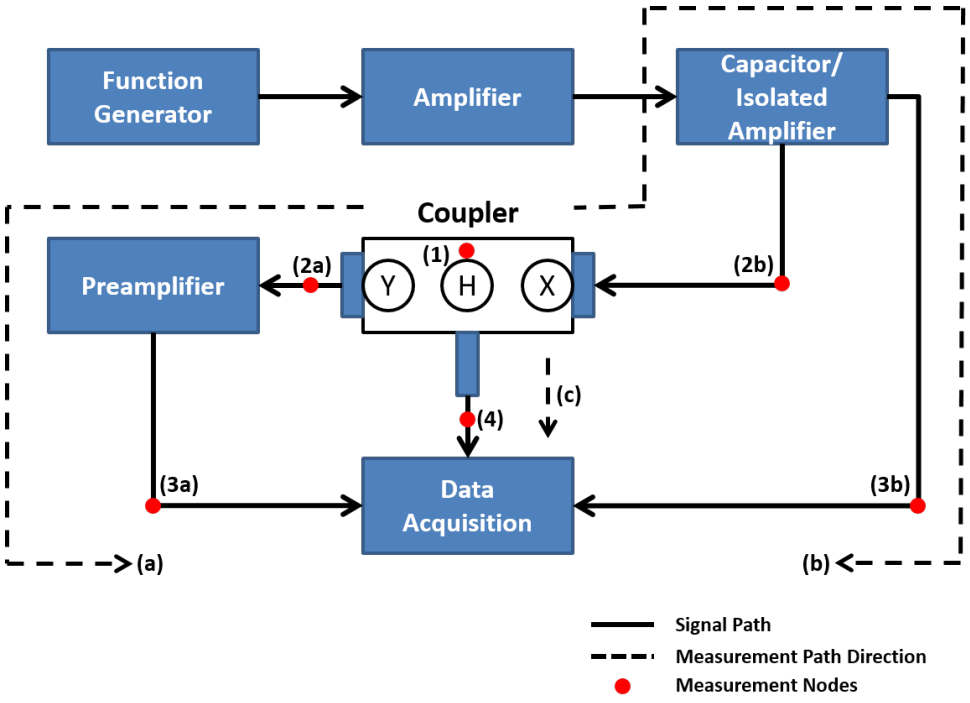

Figure 3.2. Reciprocity coupler system block diagram with measurement nodes indicated by red dots and phase changes indicated by dotted lines

Three measurement pathways through the electro-acoustic system are of interest: (a), (b), and (c). Each one begins at measurement node (1) in the fluid in the coupler cavity at the face of the hydrophone and ends at measurement node (4) where the hydrophone output voltage is recorded at the data acquisition system. Pathway (a) leads from the fluid in the coupler cavity through the receiving reciprocal transducer (Y in Figure 3.2), preamplifier, and data acquisition system. Pathway (b) leads from the fluid in the coupler cavity through the transmitting reciprocal transducer (X in Figure 3.2), capacitor/isolated amplifier, and data acquisition system. The complex gain through pathway (a) or (b) will satisfy

$$\boldsymbol{G_{tot}} = \boldsymbol{G}_{1-2m} \cdot \boldsymbol{G}_{2-3m} \cdot \boldsymbol{G}_{3-4m}, \tag{3.12}$$

where subscript number signify the nodes the complex gains act between and m can signify pathway (a) or (b). The gain magnitudes satisfy

$$G_{totm} = G_{1-2m} \cdot G_{2-3m} \cdot G_{3-4m} \tag{3.13}$$

and phases satisfy

$$\phi_{totm} = \phi_{1-2m} + \phi_{2-3m} + \phi_{3-4m}. \tag{3.14}$$

The change in phase in pathway (c), the unknown hydrophone phase response, is the phase of the complex sensitivity of the hydrophone calculated in Equation 2.18 where the signals recorded at measurement nodes (3a), (3b), and (4) are $\boldsymbol{e_{YX}}$, $\boldsymbol{e_{CX}}$, and $\boldsymbol{e_{CX}}$, respectively. The other parameters in Equation 2.18 are recorded separately when the measurements are repeated with the preamplifier connected to transducer X and the capacitor/isolated amplifier connected to transducer Y (not shown in Figure 3.2). The phase change, ϕ_{totm} for pathways (a) and (b) must be calculated and applied as a systematic phase correction to the signal measured at nodes (3a) and (3b) before they are used in Equation 2.18.

The following subsections discuss each of the complex gain terms.

$\boldsymbol{G_{1-2m}}$

As the signal passes from measurement node (1) in the coupler fluid to measurement node (2a) or (2b), the voltage output and current input to transducer Y and X, respectively, it is modified by the complex gain represented by the receiving sensitivity and transmitting

current response of reciprocal transducers Y and X. These gain and phase changes will not affect the hydrophone sensitivity calculation because the reciprocity method allows the complex receiving sensitivities and transmitting current responses of the reciprocal transducers to be rewritten in terms of the reciprocity parameter, which is equal to purely acoustic properties of the coupler, as shown in Equations 2.1-2.6.

G_{2-3m}

As the signal passes from measurement nodes (2a)/(2b), the electrical output/input to the reciprocal transducers, to (3a)/(3b), the outputs of signal amplification equipment, a complex gain is applied equal to the complex response of the amplifying equipment. The preamplifier and isolated amplifier are both unity gain, but they do shift the phase of the signals they amplify. To measure phase change ϕ_{2-3a}, the phase response of the preamplifier was measured. The phase response of the Ithaco preamplifier is shown in Figure 3.3 and is nearly flat within the ±0.5°accuracy of the HP35565A used to make the measurement.

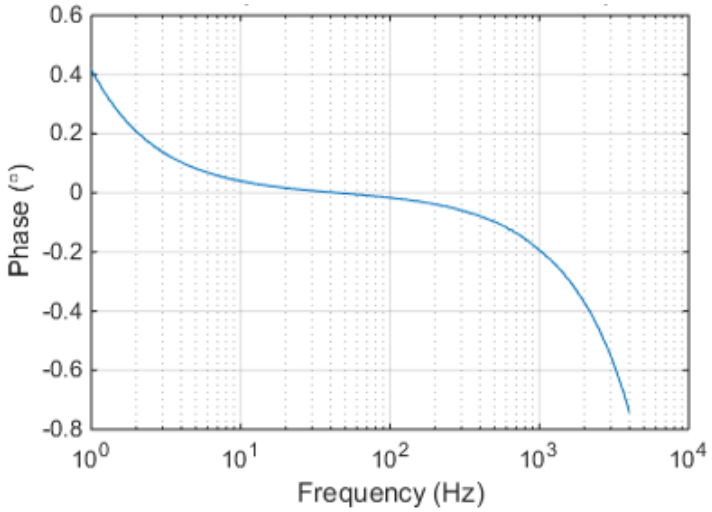

Figure 3.3. Ithaco 1201 frequency response

The same procedure used to measure ϕ_{2-3a} is applied to the standard capacitor/differential amplifier package to measure phase change ϕ_{2-3b}. The standard capacitor is wired in series with the projector. The isolated amplifier measures the voltage across the current-measuring capacitor. The phase response of interest is that between the signal leaving the

capacitor for the projector and the amplified voltage signal measured across the capacitor at the isolated amplifier output. The package has three accessible ports: the input to the standard capacitor (C_{in}), the output from the standard capacitor to the projector (C_{out}), and the voltage measurement output from the isolated amplifier (V_{out}). The response of interest ($\frac{C_{out}}{V_{out}}$) could not be measured directly with the available equipment, so two responses were measured: (1) injecting a signal into the capacitor input and measuring the signal at the amplifier voltage measurement output ($\frac{V_{out}}{C_{in}}$) and (2) injecting a signal into the capacitor input and measuring the signal at the capacitor output ($\frac{C_{out}}{C_{in}}$). Dividing the two produces the desired frequency response given by the equation below and shown in Figure 3.4.

$$\frac{\frac{C_{out}}{C_{in}}}{\frac{V_{out}}{C_{in}}} = \frac{C_{out}}{V_{out}}. \tag{3.15}$$

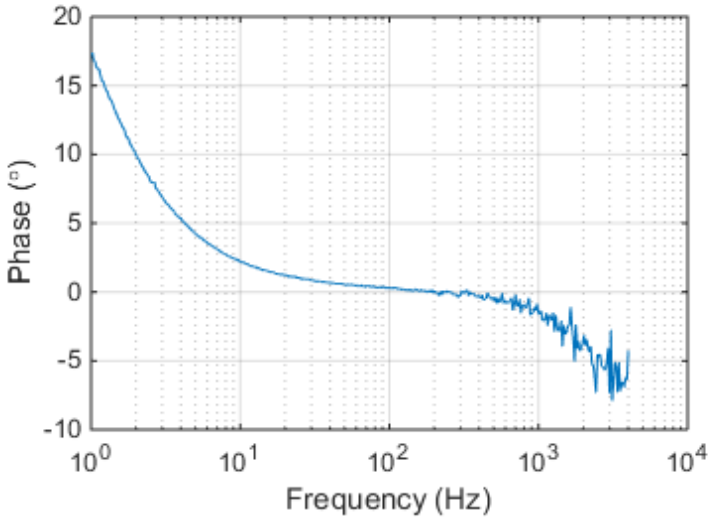

Figure 3.4. Frequency response of standard capacitor/isolated amplifier package

G_{3-4m}

As the signals pass from measurement nodes (3a)/(3b), each at a different channel of the data acquisition system, to node (4), they are subject to a complex gain that represents

magnitude and phase changes that occur due to unequal treatment of the signals at different channels. It is assumed that there is no change applied to the magnitude of the recorded signals from one channel to the next, but the same is not true for phase as the channels are not recorded simultaneously. Inspecting Equation 2.18, however, shows that any pair of equal and opposite phase adjustments ($e^{i\theta}$ terms) made to signals from the reciprocal transducers in the denominator will cancel. The data acquisition system records samples from channels sequentially from the first to the last active channel, then repeats. With the hydrophone positioned in channel two, the voltage from the receiving reciprocal transducer in channel one, and the voltage from the current measuring capacitor in channel three, phase changes imparted by the data acquisition system will be made in equal and opposite amounts to the reciprocal transducer measurements in the denominator of Equation 2.18. Therefore ϕ_{3-4a} and ϕ_{3-4b} cancel out.

If the channels on the data acquisition box, an NI-6259, cannot be arranged symmetrically around the hydrophone input channel, the time difference between channel scans can be measured and the associated phase correction applied. The NI-6259 times acquisition using the sample clock for sample rate and the convert clock to time the sequential scans over the active channels within each sample. The driver software places 10 μs of padding between channel scans unless there is not enough time between samples to pad between each active channel, at which point the channel scans are divided equally over the time period between samples. Using three active channels with the sample rate set to five times the signal frequency, the coupler measurements all receive 10 μs padding between channels from 1 Hz to 2 kHz. This padding has the desirable effect of eliminating measurement error due to settling time in the NI-6259, which (time) ranges from 1-2 μs [10]. The padding time was measured by placing a T-fitting on the signal output of the function generator and recording the function generator signal in two adjacent channels of the NI-6259. Dividing the phase difference between the two recorded signals by the frequency gave an average time delay between channels of 11 μs: 10 μs padding and 1 μs to record the measurement. Over the 5 Hz–2 kHz range of the H48 hydrophone, the associated delay between channels was constant.

3.3.2 Systematic error from compliant transducers and coupler walls

The acoustic compliance found in Equation 2.17 was derived assuming that the transducers were rigid. In actuality, transducer compliance adds a small amount to the acoustic compliance term. The acoustic compliance of the transducers can be calculated using the change in outer radius for a thick walled hollow sphere for a change in external pressure, given by [11]:

$$\Delta a = \frac{-qa}{E}\left(\frac{(1-\nu)(b^3+2a^3)}{2(a^3-b^3)} - \nu\right), \tag{3.16}$$

where Young's Modulus, E, is $6.45 \times 10^{10}\ N/m^2$ for Navy Type I lead-zirconate-titanate, Poisson's ratio, ν, is 0.343, and the inner and outer radii, a and b, are 9.53 mm and 12.7 mm, respectively. Using $q = 1$ Pa to calculate the change in radius per Pa, the compliance, or change in volume per Pa of the two reciprocal transducers and reference hydrophone are each $4.12 \times 10^{10}\ m^3/Pa$, adding $1.236 \times 10^{-15}\ m^3/Pa$ to the overall coupler compliance [9].

The compliance of the coupler wall, also assumed to be rigid, introduces error into the measurement. The coupler wall compliance was estimated using a finite element model [12] to be $2.66 \times 10^{-15}\ m^3/Pa$ with an estimated uncertainty of $\pm 2.7 \times 10^{-16}$. A check on the finite element analysis can be calculated using Equations 3.17 and 3.18 from [11],

$$\Delta b = \frac{qb}{E}\frac{a^2(1+\nu) + b^2(1-2\nu)}{a^2-b^2} \tag{3.17}$$

and

$$\Delta l = \frac{ql}{E}\frac{b^2(1-2\nu))}{a^2-b^2}, \tag{3.18}$$

to determine the change in volume of a cylindrical chamber under internal pressure, assuming the ends of the cylinder are rigid.

The coupler chamber is made of type 304 stainless steel, with a Young's modulus, E, of $1.903 \times 10^{1}1\ N/m^2$ and Poisson's ratio, ν, of 0.305. The main cylindrical portion of the coupler is 86.77 mm long, l, with an inner radius, b, of 22.23 mm. Since the coupler has a rectangular cross section, a mean outer radius, a, of 61.32 mm is used to calculate an equivalent cylinder wall thickness. The compliance contribution of the main cylindrical portion, calculated as the difference in volume per unit of applied internal pressure ($q = 1$ Pa), is $2.252 \times 10^{-15}\ m^3/Pa$. The contribution of the cylindrical side arm

that contains the hydrophone can be calculated by multiplying the main cylinder compliance by the ratio of the total volume to the main cylinder volume without transducers installed: $1.530 \times 10^{-4} m^3$ and $1.347 \times 10^{-4} m^3$, respectively. The total compliance, accounting for the hydrophone side arm is therefore $2.559 \times 10^{-15} m^3/Pa$, which agrees with the finite element analysis within the modeling uncertainty [9].

The compliance of the transducers and coupler walls add to the castor oil compliance to give the total compliance value that should be used to calculate the hydrophone sensitivity, $5.643 \times 10^{-14} m^3/Pa$. Equation 2.19 assumes only the castor oil has a compliance, so this addition is equivalent to multiplying Equation 2.8 by the factor

$$F_{\mathrm{A}} = \sqrt{\frac{\rho c^2}{\rho c^2 + C_T}}, \tag{3.19}$$

where C_T is the compliance of the transducers and coupler walls. This correction amounts to between 0.25 and 0.33 dB over the temperature and pressure range of the H48 calibration [9].

3.3.3 Wavelength correction factor

In developing the sensitivity equation for the coupler, it was assumed that pressure was constant everywhere in the coupler. This statement is a good approximation, but at higher frequencies there will be a non-negligible pressure variation across the coupler. This variation can be estimated by assuming the coupler in Figure 2.3 behaves as an acoustic waveguide where sound travels along the x direction as a plane wave and following the same procedure Zalesak uses to derive the wavelength dependent correction factor [9]. The acoustic pressure variation within the coupler is estimated as described earlier (Section 2.3), so Equations 2.10 and 2.11 still apply. Assuming $U_1 = 0$, the coefficient B was already determined to be 0. Now to solve for A, we again put

$$U_2 = -Su(L, t). \tag{3.20}$$

Applying this boundary condition to Equation 2.11, neglecting the time dependence term, and solving for A, we get

$$A = \frac{-j\omega\rho U_2}{kS\sin(kL)} = -j\frac{\rho c}{S}\frac{1}{\sin(kL)}, \tag{3.21}$$

and Equation 2.10 becomes

$$p = \frac{-j\omega\rho U_2}{kS\sin(kL)}\cos(kx) = -j\frac{\rho c}{S}\frac{\cos(kx)}{\sin(kL)}. \tag{3.22}$$

The expression for the pressure in the coupler at very low frequency ($kL << 1$), where the pressure does not vary over the length of the coupler can be derived from Equation 3.22 using small angle approximations for the trigonometric functions,

$$p_{lf} = \frac{-j\rho c U_2}{SkL} = \frac{\rho c^2}{j\omega V}U_2, \tag{3.23}$$

where the volume of the coupler, V, is equal to SL. Note that $V/\rho c^2$ is the acoustic compliance of the coupler. Since the measured pressures are affected by this small variation across the coupler, they must be converted to low-frequency pressures to preserve the constant pressure assumption required in Equation 2.18 by multiplying by the ratio p_{lf}/p. Dividing Equation 3.23 by Equation 3.22, we get this ratio, the correction factor F:

$$F = \frac{p_{lf}}{p} = \frac{\sin(kL)}{kL\cos(kx)}. \tag{3.24}$$

Zalesak [9] adds one additional refinement to the correction. In the actual coupler, the transducers do not form the walls at each end of the coupler, but are offset a small distance inward. He accounts for this difference by assuming that the coupler reciprocal transducers are infinitesimally thin and span the coupler cross section at a distance d from each wall of the coupler. Figure 3.5 shows these assumptions with the projecting transducers located at $x = L - d$ and the receiving transducer at $x = d$. Applying the same low-frequency pressure assumption and ratio gives his wavelength dependence correction factor, F_2, given by

$$F_2 = \frac{\sin(kL)}{kL\cos(kd)\cos(kx)}. \tag{3.25}$$

The additional $\cos(kd)$ term in the denominator improves the accuracy of F_2. F and F_2 are within 10% of each other over the H48 hydrophone frequency range 1-2000 Hz. Zalesak does not add any more features to the wavelength dependent correction analysis, although Figure 3.5 is still missing some features of the coupler. The reciprocal transducers located a distance d from each wall are actually 2.54 cm diameter spheres and the coupler cross section

is not constant — there is a small perpendicular leg in the middle, forming a T-shape where the H48 hydrophone is installed. The transducers are also assumed to be stationary. Zalesak argues that the correction is already small — for the H48 coupler, its maximum value is 0.06 dB at 2000 Hz, falling to 0.01 dB at 700 Hz — and that further refinements would only make relatively small adjustments to the correction and are therefore negligible [9]. But additional refinements could be made using a lumped parameter, or more accurately, a finite element model.

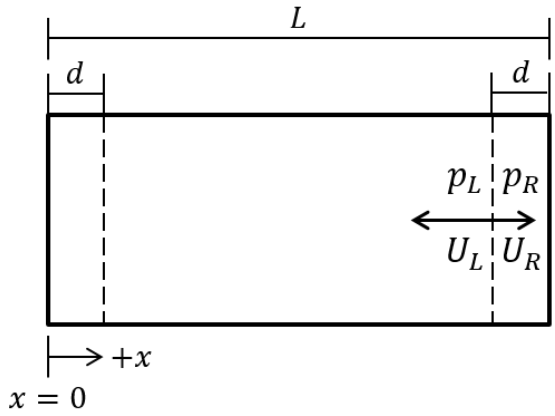

Figure 3.5. Illustration of Zalesak's coupler configuration assumptions for the wavelength dependent correction factor

The ratio calculated to correct the measured pressures also applies to the measured voltage magnitudes. Two voltage measurements must be corrected: the hydrophone voltage and the receiving transducer voltage. The hydrophone voltage correction is given by Equation 3.25 using $x = L/2$:

$$F_{2\mathrm{H}} = \frac{\sin(kL)}{kL\cos(kd)\cos\left(\frac{kL}{2}\right)} = \frac{2\sin\left(\frac{kL}{2}\right)}{kL\cos kd}. \tag{3.26}$$

The receiving transducer voltage correction is also given by Equation 3.25 using $x = d$:

$$F_{2\mathrm{T}} = \frac{\sin(kL)}{kL\cos^2(kd)}. \tag{3.27}$$

3.4 H48 Hydrophone Low-Frequency Equivalent-Circuit Model

The behavior of the H48 hydrophone at low frequency, far below its first resonance, can be approximated as an RC high-pass filter circuit [13], shown in Figure 3.6. V is the open circuit voltage generated at the hydrophone, C the hydrophone capacitance, R the input resistance to the preamplifier, G the gain of the preamplifier, and V_{out}, the voltage output of the preamplifier. The response of the RC circuit is given by

$$\boldsymbol{M} = \frac{\boldsymbol{V_{out}}}{V} = \frac{V \times G}{1 + 1/j\omega\mathrm{RC}} \tag{3.28}$$

and the phase angle by

$$\phi = \tan^{-1}\left(\frac{1}{\omega\mathrm{RC}}\right) = \tan^{-1}\left(\frac{f_0}{f}\right). \tag{3.29}$$

The cutoff frequency, f_0, is given by

$$f_0 = \frac{1}{2\pi\mathrm{RC}}. \tag{3.30}$$

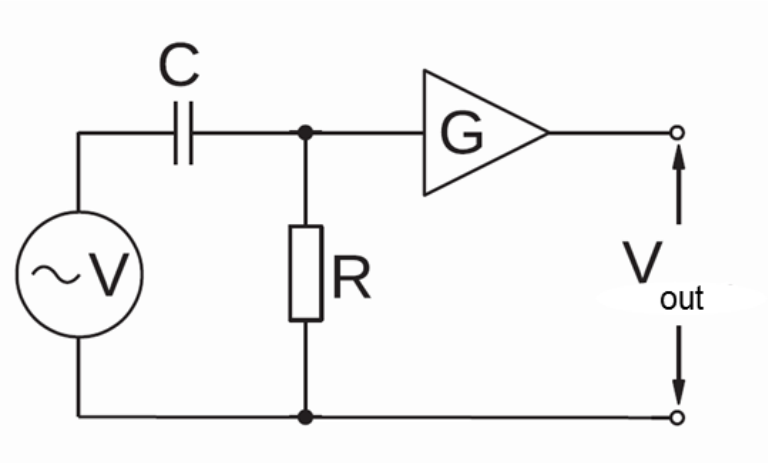

Figure 3.6. Simplified hydrophone circuit model. Adapted from [13].

At the cutoff frequency, the sensitivity magnitude is -3 dB from its flat, high-frequency value and the phase is 45°. The low-frequency roll-off of the circuit is shown in Figure 3.7. Note that the magnitude response flattens out about one decade above the cutoff frequency, but

the phase does not flatten out until about two decades above the cutoff frequency. The low-frequency cutoff or 3 dB-down frequency of the H48 reference hydrophone was designed to be 0.035 Hz, but, after construction, was measured to be 0.08 Hz [14]. This (0.08 Hz) cutoff frequency implies that the phase response would begin to fall off below 8 Hz. At 1 Hz, the phase should be about 18°.

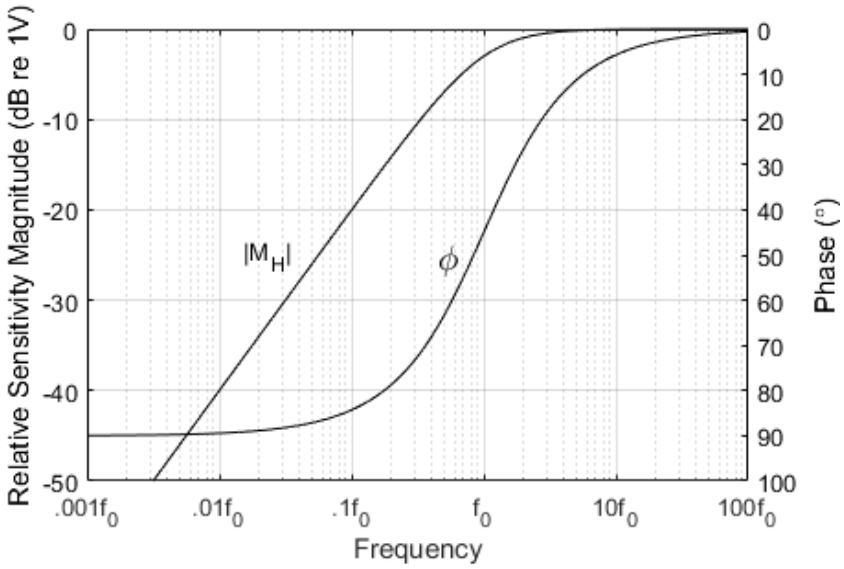

Figure 3.7. Magnitude and phase roll-off at low frequency. Adapted from [15].

The simple RC high-pass filter model was fit to the complex sensitivity data using a nonlinear least-squares curve fitting procedure. For a given data set of input frequencies and complex sensitivity data, two fitting parameters were calculated from Equation 3.28, the voltage/gain product, $V \times G$, and the RC time constant, RC. An unweighted, complex Levenberg-Marquardt algorithm was used, which, as implemented in Matlab's *lsqnonlin* function [16], allows the least squares coefficients to be fit in the complex plane without having to separate their real and imaginary parts in the objective function. To allow for resistive and capacitive losses, the RC parameter was allowed to be complex, but the gain term was restricted to be a real number, as more detailed treatment of the preamplifier is left to future work. The fitted parameters were used to estimate the complex sensitivity, from which the the magnitude and phase were estimated by taking the respective magnitude and angle of the real and imaginary parts of the sensitivity estimate.

3.5 Procedure

A complex-valued H48 coupler reciprocity calibration was performed across frequency, temperature, and pressure in accordance with [17]. Pressure was varied from 50 to 2000 psi. Temperature was varied from 0°C to 40°C. For this report, at each temperature and pressure, a logarithmic frequency sweep was performed from 1-2000 Hz. At each frequency, 20 cycles of the time series signals were recorded at a sample rate of five times the signal frequency. Each frequency sweep was repeated ten times.

CHAPTER 4:
Uncertainty Estimation

The new complex coupler reciprocity calibration procedure must account for the uncertainties treated by Zalesak [9] along with uncertainty in the phase response of the coupler components, the electronic equipment in the signal paths, the NI-6259 data acquisition hardware, and the effect of random error in calculating the complex sensitivity. The uncertainty is split into the two types described in the National Institute of Standards and Technology (NIST) guidelines for evaluating uncertainty [18], A and B. NIST type A uncertainty is calculated by performing statistical calculations on measurements. NIST type B covers uncertainties calculated in any other way, such as factoring in the accuracy of equipment used to make measurements or parameters used to calculate results.

4.1 Estimation of NIST Type A Uncertainty

Uncertainty in the complex sensitivity produces magnitude and phase uncertainty. Unlike measurements that fall into the set of real numbers, magnitudes must be greater than zero and phases fall in the range of -π to π, which is problematic for the arithmetic involved in uncertainty calculations. Analyzing the uncertainty in the complex plane, where the real and imaginary axes extend to positive and negative infinity avoids these problems [19]. Only after the uncertainties of the real and imaginary parts of the complex sensitivity are calculated are they converted to magnitude and phase uncertainties.

The random error in the complex sensitivity is estimated using a bivariate normal distribution that accounts for the uncertainty in each of the real and imaginary parts as well as the correlation between the two, represented by a covariance matrix. Using singular value decomposition, the eigenvalues and eigenvectors of the covariance matrix can be used to define an elliptical region of uncertainty in the complex plane [19]. An example from an H48 data set is shown in Figure 4.1. The plot shows the real and imaginary parts of ten measurements of the complex sensitivity recorded at a single frequency. This data group and confidence region represent one of the data groups and confidence regions found in Figure 5.1, a data set recorded across the frequency range 5 Hz - 2 kHz. The lengths of the

major and minor semiaxes are related to the eigenvalues of the covariance matrix, and the rotation angle is determined by the correlation of the real and imaginary parts. The length of the major semiaxis, a, is given by the largest eigenvalue and the minor semiaxis, b, by the smallest, as shown in Equations 4.1 and 4.2:

$$a = \sqrt{s\lambda_{max}}\,, \tag{4.1}$$

$$b = \sqrt{s\lambda_{min}}\,, \tag{4.2}$$

where s is a coverage factor given by

$$s = \sqrt{\frac{2(n-1)}{n-2}F_{2,n-2}(\alpha)}\,, \tag{4.3}$$

determined by the $F_{2,n-2}$ inverse cumulative distribution function with two degrees of freedom and n observations at a level of confidence α [20]. The $F_{2,n-2}$ is used instead of the standard normal distribution used for scalar measurements, resulting in coverage factors different than those used for scalar measurements, (i.e., k = 1.96 for 95% confidence). The ellipse in Figure 4.1 is scaled using Equation 4.3 with a 95% confidence interval resulting in a coverage factor of 2.45 for 1000 observations. The major axis of the ellipse is rotated from the real axis by the angle between the largest eigenvector of the covariance matrix and the real axis [21].

The uncertainty in the magnitude and phase can be calculated from the magnitude and phase boundary points on the covariance ellipse shown in Figure 4.1. The magnitude boundary points are selected to give the longest and shortest phasors (from the origin to the covariance ellipse boundary) and the phase boundary points, to give the smallest and largest possible angles from a phasor on the covariance ellipse boundary to the real axis. These minimums and maximums were calculated using *fminbnd* in Matlab and are used to define the uncertainty at a particular frequency. The magnitude and phase errors across the frequency range are shown in Figure 4.2.

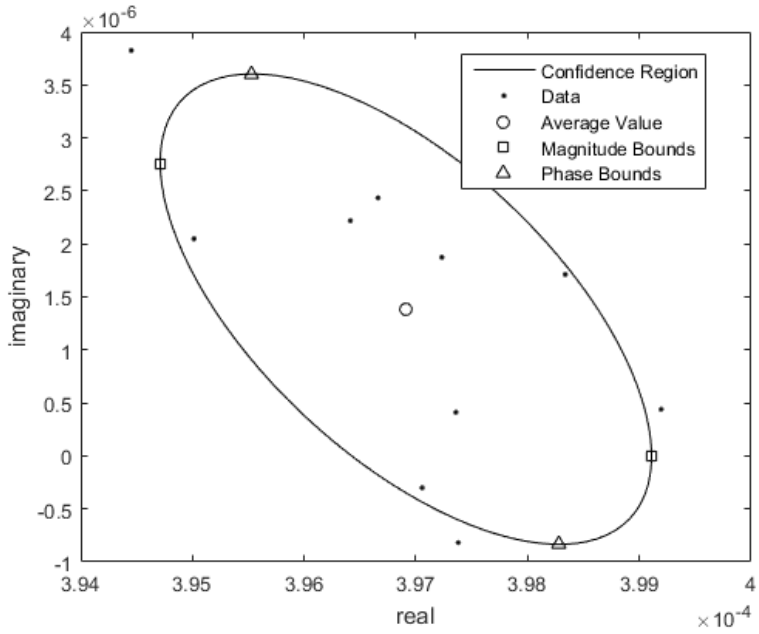

Figure 4.1. An example covariance ellipse showing a 95% confidence region around a group of H48 complex sensitivity measurements at a constant frequency

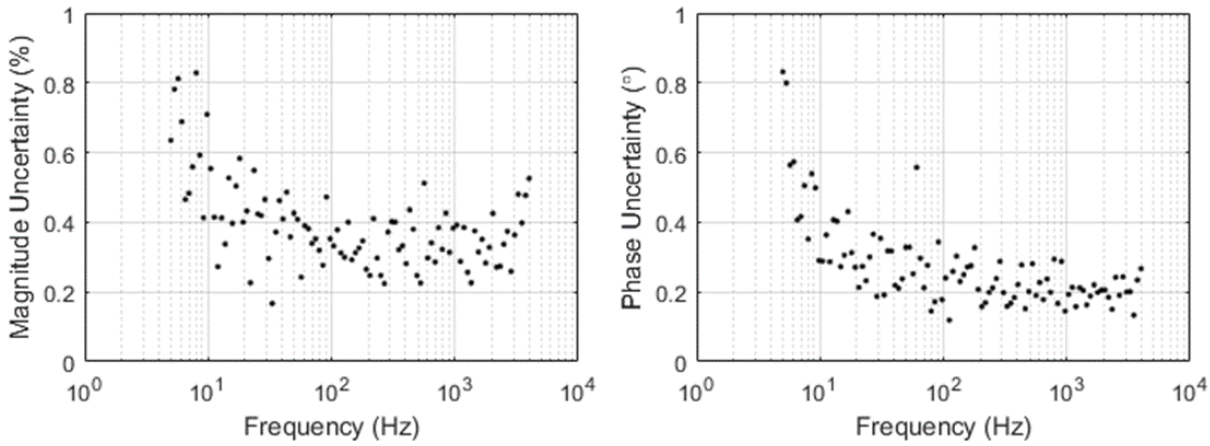

Figure 4.2. Magnitude and phase random errors across frequency

4.2 Estimation of NIST Type B Uncertainty

Random error from the complex voltage measurements contributes to uncertainty in the magnitude and phase of the sensitivity, but other factors will contribute additional uncertainty. The total phase uncertainty is that calculated from the covariance matrix depicted in Figure 4.2, combined with the uncertainty in the phase measurements taken with the HP35565 signal analyzer, ±0.5°, used to correct for the phase shift in the differential amplifier,

$$\delta\phi_{tot} = \sqrt{\delta\phi_{rand}^2 + 0.5^2}. \tag{4.4}$$

The final magnitude uncertainty is a combination of uncertainties calculated from the covariance matrix and additional uncertainties from measured quantities in Equation 2.18, as shown in Equation 4.5 (complex values assumed here):

$$\frac{\delta|\boldsymbol{M_H}|}{|\boldsymbol{M_H}|}_{total} = \sqrt{\left(\frac{\delta|\boldsymbol{M_H}|}{|\boldsymbol{M_H}|}\right)_{cov}^2 + \left(\frac{\delta|\boldsymbol{M_H}|}{|\boldsymbol{M_H}|}\right)_{add}^2}. \tag{4.5}$$

The additional uncertainty term can be broken into electrical and acoustic compliance groupings, with an uncertainty term assigned for each parameter in Equation 2.18.

In the electrical group, the uncertainties in voltage measurements from the hydrophone, $\delta\boldsymbol{e_{HX}}$ and $\delta\boldsymbol{e_{HY}}$ arise from the accuracy limitation of the NI-6259 used to make the voltage measurements. The uncertainties in voltage measurements from the receiving reciprocal transducers, $\delta\boldsymbol{e_{XY}}$ and $\delta\boldsymbol{e_{YX}}$, arise from the accuracy limitation of the NI-6259 along with the gain accuracy of the Ithaco 1201 preamplifier used to amplify the signal in front of the NI-6259. The uncertainties in voltage measurements across the standard capacitor, $\delta\boldsymbol{e_{CX}}$ and $\delta\boldsymbol{e_{CY}}$, also arise from the accuracy limitation of the NI-6259 with an additional contribution from the differential amplifier used amplify those signals. Finally, the uncertainty in the capacitance of the standard capacitor as manufactured, δC_p must be accounted for. These terms are explained in more detail in Section 4.2.1.

In the acoustic compliance group, there is uncertainty in the volume of the coupler cavity, δV, associated with the method used to measure that volume. The uncertainty in the speed of sound in castor oil, δc, arises from uncertainties in the estimate of that value [22] and in the uncertainty in the temperature and pressure inside the coupler cavity. The uncertainty in

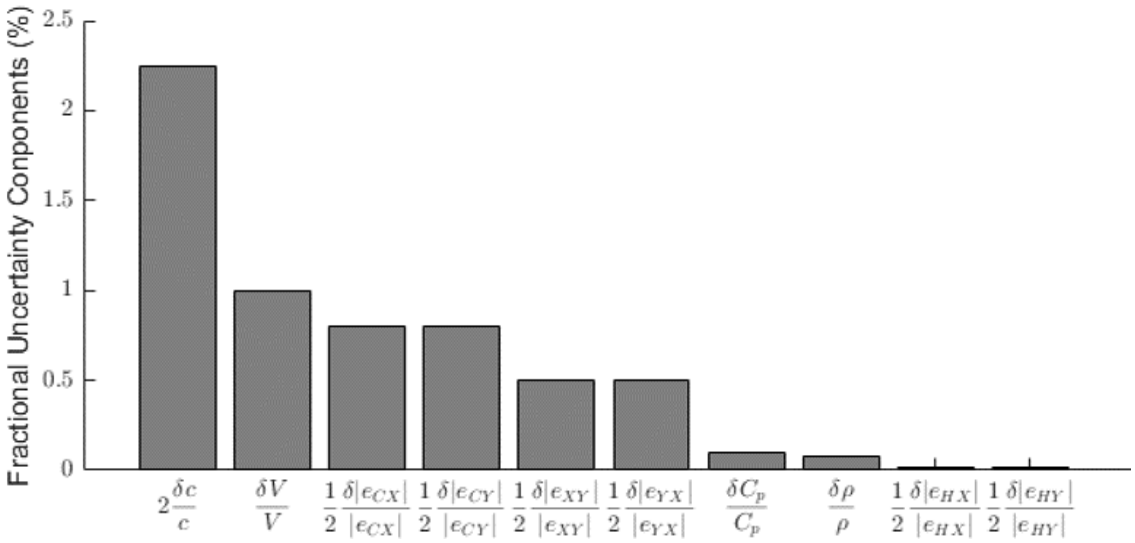

Figure 4.3. Components of fractional uncertainty in the sensitivity magnitude from Equation 4.6, taken from a data set at 1000 psi and 3.2°C

the density of castor oil, $\delta\rho$, also arises from the uncertainty in the temperature and pressure inside the coupler cavity. These terms are explained in more detail in Section 4.2.2.

The size of the fractional uncertainty magnitudes of each of these additional uncertainties as components of the sensitivity magnitude uncertainty are shown in Figure 4.3, based on the relationships of the quantities in Equation 2.18. The fractional uncertainty in the sound speed dominates and can be as high as 3% at the top of the temperature range (note that the effect of the fractional uncertainty in the sound speed is doubled). The volume fractional uncertainty is less than half the amount of the sound speed. The fractional uncertainties in the voltages measured across the standard capacitor are a close third, despite their contribution being reduced by half. Those voltage uncertainties are dominated by the 1.6% measurement error in the differential amplifier. Similarly the next largest fractional uncertainty, that of the receiving reciprocal transducer measurement, is dominated by the 1% error in the gain of the Ithaco 1202 preamplifier. The fractional uncertainty in the capacitance of the standard capacitor used in the current measurement is given by the manufacturer to be 0.1%. The smallest contribution comes from the fractional uncertainty of the hydrophone voltages measured by the NI-6258.

These additional fractional uncertainties can be combined in quadrature for a total additional fractional uncertainty of 1.4%, as shown in Equation 4.6:

$$\frac{\delta|\boldsymbol{M_H}|}{|\boldsymbol{M_H}|}_{add} = \frac{1}{2}\left(\left(\frac{\delta|\boldsymbol{e_{HX}}|}{|\boldsymbol{e_{HX}}|}\right)^2 + \left(\frac{\delta|\boldsymbol{e_{HY}}|}{|\boldsymbol{e_{HY}}|}\right)^2 + \left(\frac{1}{2}\frac{\delta|\boldsymbol{e_{YX}}|}{|\boldsymbol{e_{YX}}|}\right)^2 + \left(\frac{1}{2}\frac{\delta|\boldsymbol{e_{XY}}|}{|\boldsymbol{e_{XY}}|}\right)^2 + \left(\frac{1}{2}\frac{\delta|\boldsymbol{e_{CX}}|}{|\boldsymbol{e_{CX}}|}\right)^2 + \left(\frac{1}{2}\frac{\delta|\boldsymbol{e_{CY}}|}{|\boldsymbol{e_{CY}}|}\right)^2 + \left(\frac{\delta V}{V}\right)^2 + \left(\frac{\delta\rho}{\rho}\right)^2 + \left(2\frac{\delta c}{c}\right)^2 + \left(\frac{\delta C_p}{C_p}\right)^2\right)^{\frac{1}{2}}. \quad (4.6)$$

4.2.1 Uncertainty in the measured voltage magnitudes

The magnitude of the voltage terms e_{HX}, e_{HY}, e_{XY}, e_{CX}, e_{YX}, and e_{CY} all contain uncertainty due to the absolute accuracy of the NI-6259, which varies with temperature and can be calculated from the NI-6259 specifications [10] as shown in Equation 4.7:

$$\text{Accuracy}_{\text{NI-6259}} = V_{meas}(\text{gainErr}) + \tfrac{1}{2}(\text{offsetErr}) + \text{noiseErr}. \quad (4.7)$$

For the coupler measurement setup, this uncertainty is split roughly equally into an offset error, offsetErr, and gain error, gainErr, with gain error being slightly smaller at room temperature. The constant $1/2$ is selected from a chart of values in [10] and changes based on the selected input range in the NI-6259. For the number of readings averaged for each voltage measurement, the noise error term is negligible. Offset and gain errors are shown in Equations 4.8 and 4.9.

$$\text{gainErr} = 80\text{ppm} + \left(13\frac{\text{ppm}}{^\circ\text{C}} \times \text{TempDrift}\right) + \left(1\frac{\text{ppm}}{^\circ\text{C}} \times \text{CalTempDiff}\right) \quad (4.8)$$

$$\text{offsetErr} = 20\text{ppm} + \left(27\frac{\text{ppm}}{^\circ\text{C}} \times \text{TempDrift}\right) + 60\text{ppm} \quad (4.9)$$

TempDrift is the change in temperature since the last internal calibration. The NI-6259 can perform an internal calibration on command that resets this temperature difference, which can be performed at the start of each day's measurements. Therefore TempDrift amounts to the change in temperature in the coupler lab over the course of the day's measurements. CalTempDiff is the difference in temperature between the coupler lab and the lab at National Instruments where the NI-6259 was originally calibrated. Note that the constants are selected from a chart of values in [10] and changed based on the selected input

range in the NI-6259. The offset portion of the error depends on the selected input range (a constant) and temperature of the NI-6259. Over the short time period it takes to collect a set of measurements at one frequency, this error will tend to shift all the measurements in the same direction. The least-squares fit on that frequency data set will separate that shift into a DC offset term, which is discarded from sensitivity calculations. Therefore the offset portion of the NI-6259 uncertainty is ignored. The remaining gain portion will distort only the magnitude of the signal and will be factored in to the voltage uncertainties in Equation 4.6.

The voltage magnitudes representing the current to transducers X and Y ($|\boldsymbol{e_{CX}}|$ and $|\boldsymbol{e_{CY}}|$) have an additional uncertainty due to the differential amplifier used to make those measurements. These voltage measurements are made across a standard 1μF capacitor through a differential amplifier, as shown in the simplified circuit in Figure 4.4.

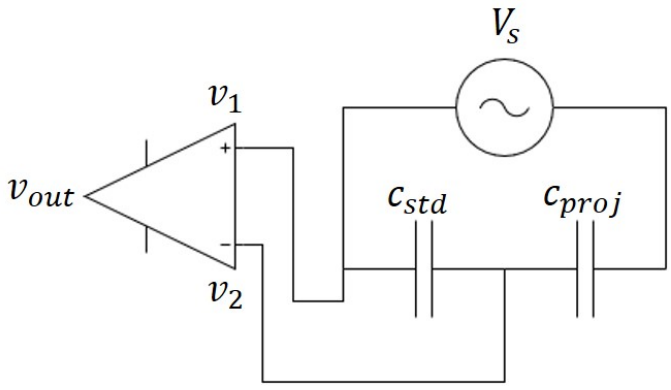

Figure 4.4. Simplified circuit of differential amplifier, standard capacitor, and projector

Given a source voltage, V_s, and a capacitance of 4.32 nF for the projector (c_{proj}) and 1μF for the standard capacitor (c_{std}), the voltage, v_{out}, measured by the differential amplifier is given in [23] as

$$v_{out} = A_d(v_1 - v_2) + A_{cm}v_{cm}\,, \tag{4.10}$$

where A_d is the differential gain, A_{cm} is the common-mode gain, and v_{cm} is the voltage common to both inputs of the amplifier, which in this case, is just v_2. From the capacitances, the voltage drop across the standard capacitor, $v_1 - v_2$, is $0.0043V_s$, and the voltage drop

across the projector, v_2, is $0.9957V_s$. The error term is the common-mode contribution to the voltage output, which can be expressed as the fractional error

$$v_{err} = \frac{A_{cm}v_{cm}}{A_d(v_1 - v_2)} \, . \tag{4.11}$$

The common-mode rejection ratio of the differential amplifier is defined in [23] as

$$\text{CMRR} = 20\log\left(\frac{A_d}{|A_{cm}|}\right) \tag{4.12}$$

and is given by the manufacturer to be -83 dB. Solving Equation 4.12 for the ratio $A_d/|A_{cm}|$ and inserting into Equation 4.11, we get a voltage error of 1.6% [9]. This uncertainty is added in quadrature with the uncertainty from the NI-6259 for these two voltage terms.

4.2.2 Uncertainty in the acoustic compliance terms

The volume, density, and sound speed terms enter the sensitivity calculation by way of the acoustic compliance term in the reciprocity parameter, introduced in Equation 2.17 and reproduced in Equation 4.13:

$$C_A = \frac{V}{\rho c^2} \, , \tag{4.13}$$

where V is the volume of the castor oil filling the coupler cavity, ρ is the density of the castor oil, and c is the speed of sound castor oil.

The fractional uncertainty in the volume is 1% [9] based on the accuracy of the original volume measurement.

The sound speed in castor oil is estimated from the empirical relation in Equation 4.14 given by Timme [22], with an absolute accuracy of ±1.1%:

$$c(T,p) = 1570(a_0 + a_1T + a_3T^3 + a_2Tp + a_4p + a_5p^2). \tag{4.14}$$

Inputs to this relation are temperature, T, in degrees Celsius, pressure, p, in MPa, and the constants a_0 through a_5 given in Table 4.1. The ambient temperature and pressure are only held constant within ±1°and ±10 psi, respectively, contributing uncertainty to the calculated

sound speed as shown in Equation 4.15:

$$\delta c(T,p) = 1570\left((a_1 + 3a_3T^3 + a_2p)\delta T + (a_2T + a_4 + 2a_5p)\delta p\right). \tag{4.15}$$

These errors do not add in quadrature as they are not independent. Changes in temperature of the coupler are directly proportional to changes in pressure within a data set. The absolute accuracy of the sound speed equation is added in quadrature to the fractional uncertainty due to temperature and pressure variation for the total fractional uncertainty in the sound speed shown in Equation 4.16:

$$\frac{\delta c}{c} = \sqrt{\left(\frac{\delta c(T,p)}{c}\right)^2 + (1.1‰)^2}. \tag{4.16}$$

Table 4.1. Constants for the empirical relationship of sound speed in castor oil with temperature and pressure

Constant	Value	Units
a_0	1	none
a_1	-2.15×10^{-3}	$\frac{1}{^\circ C}$
a_2	4.0×10^{-6}	$\frac{1}{^\circ C^2}$
a_3	2.5×10^{-6}	$\frac{1}{^\circ C \times MPa}$
a_4	2.22×10^{-3}	$\frac{1}{MPa}$
a_5	-3.0×10^{-6}	$\frac{1}{MPa^2}$

The density of castor oil is estimated by the relation given in Stallard [24] as

$$\frac{1}{\rho} = b_1 + b_2T + b_3T^2 + b_4T^3 + b_5p + b_6pT + b_7pT^2 + b_8pT^3 + b_9p^2 + b_{10}p^2T + b_{11}p^2T^2 + b_{12}p^3 + b_{13}p^3T, \quad (4.17)$$

where T is the temperature in degrees Celsius and p is the pressure in MPa. The coefficients are given in Table 4.2. As with the sound speed estimate above, uncertainty is added due to the variation of temperature and pressure within the test setup, given in Equation 4.18:

$$\delta\rho = \delta\tfrac{1}{\rho} = \left(b_2 + 2b_3T + 3b_4T^2 + b_6p + 2b_7pT + 3b_8pT^2 + b_{10}p^2 + 2b_{11}p^2T + b_{13}p^3\right)\delta T + \left(b_5 + b_6T + b_7T^2 + b_8T^3 + 2b_9p + 2b_{10}pT + 2b_{11}pT^2 + 3b_{12}p^2 + 3b_{13}p^2T\right)\delta p. \quad (4.18)$$

These errors do not add in quadrature, as changes in temperature of the coupler are directly proportional to changes in pressure.

The uncertainty in the compliance term can vary with pressure and temperature. The variation in uncertainty across the pressure range is negligible. The variation across temperature is shown in Figure 4.5.

Table 4.2. Constants for the empirical relationship of castor oil density with temperature and pressure

Constant	Value	Units
b_1	1.027	cm^3g^{-1}
b_2	7.038×10^{-4}	$cm^3g^{-1}(^\circ C)^{-1}$
b_3	9.659×10^{-7}	$cm^3g^{-1}(^\circ C)^{-2}$
b_4	3.045×10^{-9}	$cm^3g^{-1}(^\circ C)^{-3}$
b_5	-4.909×10^{-4}	$cm^3g^{-1}MPa^{-1}$
b_6	-2.633×10^{-6}	$cm^3g^{-1}MPa^{-1}(^\circ C)^{-1}$
b_7	-4.042×10^{-9}	$cm^3g^{-1}MPa^{-1}(^\circ C)^{-2}$
b_8	-8.772×10^{-11}	$cm^3g^{-1}MPa^{-1}(^\circ C)^{-3}$
b_9	1.471×10^{-6}	$cm^3g^{-1}MPa^{-2}$
b_{10}	9.181×10^{-9}	$cm^3g^{-1}MPa^{-2}(^\circ C)^{-1}$
b_{11}	3.591×10^{-11}	$cm^3g^{-1}MPa^{-1}(^\circ C)^{-2}$
b_{12}	-3.634×10^{-9}	$cm^3g^{-1}MPa^{-3}$
b_{13}	-1.657×10^{-11}	$cm^3g^{-1}MPa^{-3}(^\circ C)^{-1}$

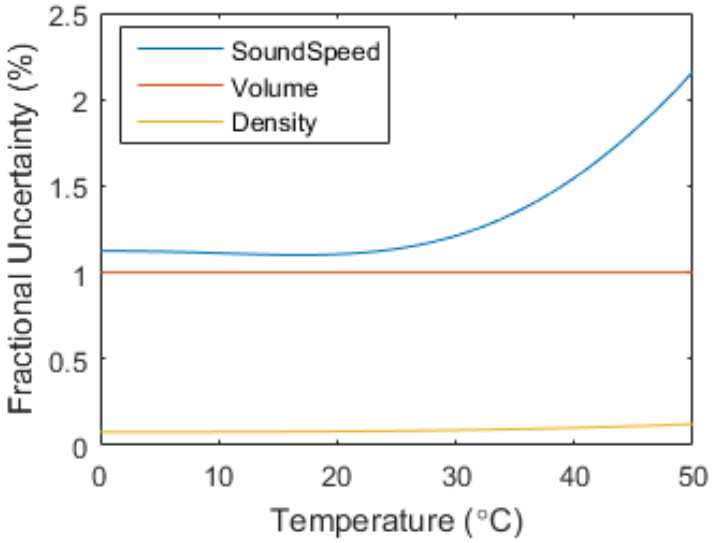

Figure 4.5. Fractional uncertainty in the components of the acoustic compliance in the calculation of sensitivity

CHAPTER 5:
Results and Discussion

The results of two complex hydrophone calibrations with systematic magnitude and phase corrections, NIST type A and B uncertainties, and fitted simple, high-pass equivalent-circuit models are presented. The complex sensitivity is plotted in the complex plane, and the magnitude and phase is plotted with respected to frequency.

The complex free-field voltage sensitivity of H48 serial number two with the associated covariance ellipses and the fitted simple, high-pass equivalent-circuit model is shown in Figure 5.1. Each ellipse represents a confidence region around the average sensitivity measurement representing the NIST type A error at a particular frequency between 5 Hz and 2000 Hz (spaced logarithmically), calculated as shown in Section 4.1. Each average measurement is the mean value of ten separate fittings of the least squares parameters to a sampled waveform. Each least squares fit is performed on data sampled at five times the signal frequency for 20 signal periods, or 100 data points. The frequencies begin at 5 Hz at the smallest values of the real and imaginary parts of the sensitivity in Figure 5.1. As frequency increases, both the real and imaginary parts of the sensitivity increase. As the imaginary part of the sensitivity approaches zero above 100 Hz, the real part decreases until the frequency reaches 2000 Hz. The model is a good fit for the data at low frequency, but fits poorly above 100 Hz, above those of primary interest in this report. The relationship between the real and imaginary parts of the complex, open-circuit voltage sensitivity are shown in Figures 5.2 and 5.3, respectively, where the frequency above which the model fit deteriorates is more apparent. More physically intuitive conclusions can be drawn from plotting the magnitude and phase of the data and model.

The magnitude portion of the free-field voltage sensitivity (FFVS) is calculated by taking the magnitude of average sensitivity values from Figure 5.1 and converting to dB re $1V/\mu Pa$. The FFVS magnitude of H48 serial number 4 is shown in Figure 5.4. The magnitude of the model is calculated in the same way from the estimated complex FFVS and converted to dB re $1V/\mu Pa$. These data can also be verified by comparison with the FFVS magnitude calculated from RMS voltage measurements made with the multimeters in a standard

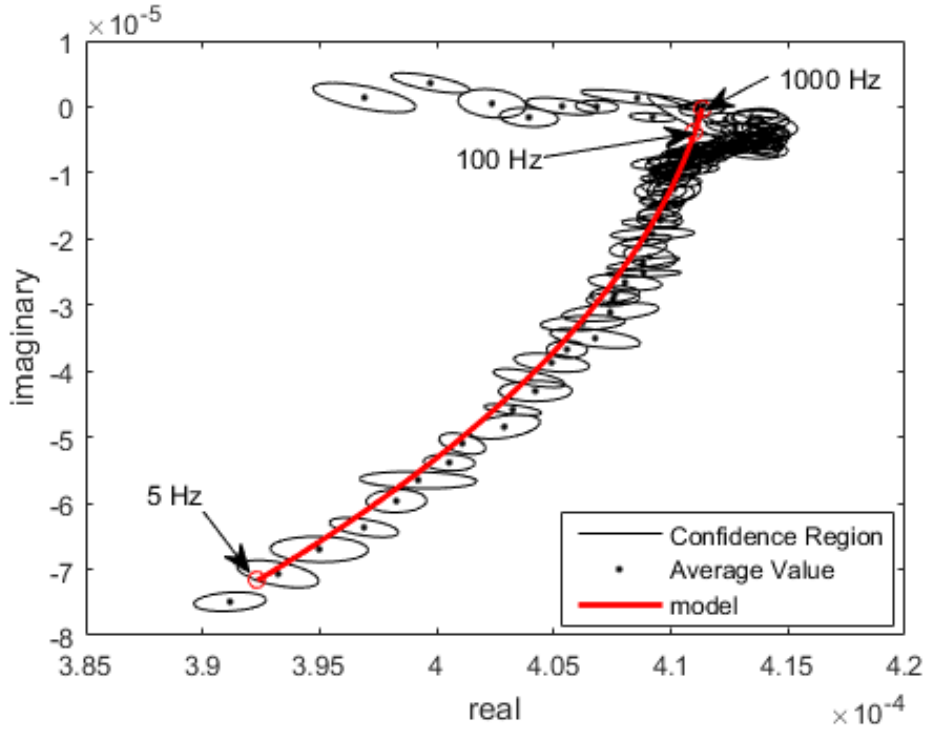

Figure 5.1. Complex open-circuit voltage sensitivity measurements and uncertainty fitted with a simple circuit model for H48, serial number two, from a data set taken at 500 psi and 39.6°C

coupler calibration [17]. The FFVS magnitudes measured from each method agree within measurement uncertainty above 15 Hz. Below 15 Hz, the signal is below the minimum frequency the HP 3478A multimeters are certified to measure, which may explain the disagreement in the data and the upward trend in the FFVS calculated from multimeter data at low frequency. This upward trend is not supported by the model nor by the H48 design document that specifies the typical FFVS for an H48 hydrophone [14]. It is not clear from the sensitivity magnitude data where the cutoff frequency is for the hydrophone. At the high end of the frequency range, both sets of measurements show a pronounced hump where the model is flat. This poor fit corresponds to the hooked section of the model in Figure 5.1.

The phase response and model are calculated by taking the angle of the complex values and their modeled estimates in Figure 5.1. The phase response of H48 serial number four is compared to the simple, high-pass equivalent-circuit model in Figure 5.5. At low and high

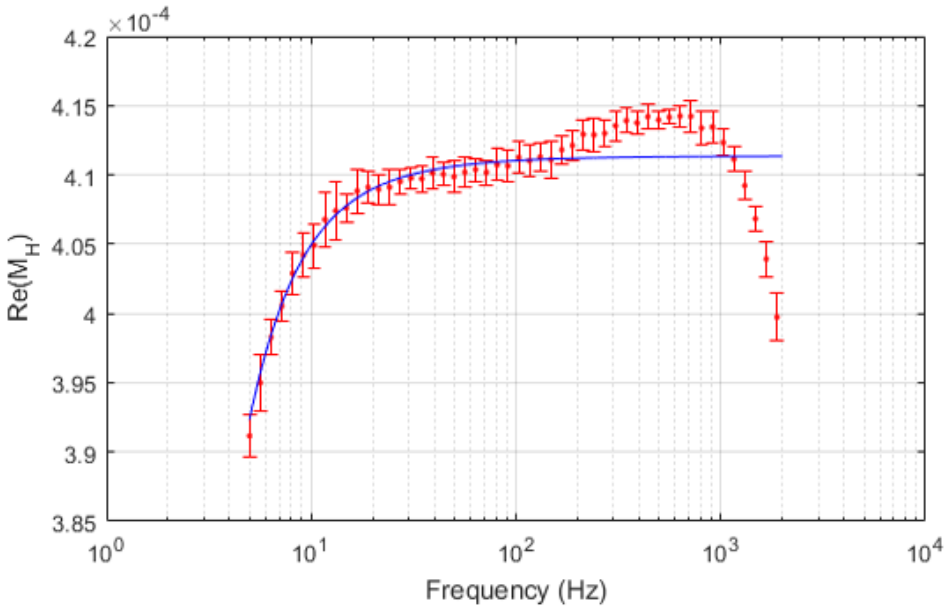

Figure 5.2. The real part of the complex open-circuit voltage sensitivity measurements plotted versus frequency with NIST type A uncertainty and the simple, high-pass equivalent-circuit model for H48, serial number 2, from a data set taken at 500 psi and 39.6°C

frequencies, the model is in good agreement with the data. In the middle of the frequency range, the phase data does not flatten out like the model. The fit in this range can be improved by letting the gain coefficient of the simple circuit model be complex, introducing a stray capacitance-like term to the input of preamplifier. This analysis is excluded, as a more detailed model of the preamplifier is left to future work.

At 1 Hz, the measured and modeled phase is 20°. It should be noted for low frequency calibrations that the constant phase assumption breaks down between 10 Hz and 20 Hz and gets increasingly worse as frequency continues to decrease. Since the phase begins its roll-off at a higher frequency, it is easier to calculate the cutoff frequency with these data than with the magnitude data alone. Extrapolating with the model to a phase of 45°, we get an estimated cutoff frequency of 0.3 Hz, higher than the 0.08 Hz measured when the H48 hydrophones were built [14]. Assuming even 10° of error in the model extrapolated down to 0.3 Hz gives an uncertainty in the estimated cutoff frequency of 0.1 Hz, as seen in Figure 3.7.

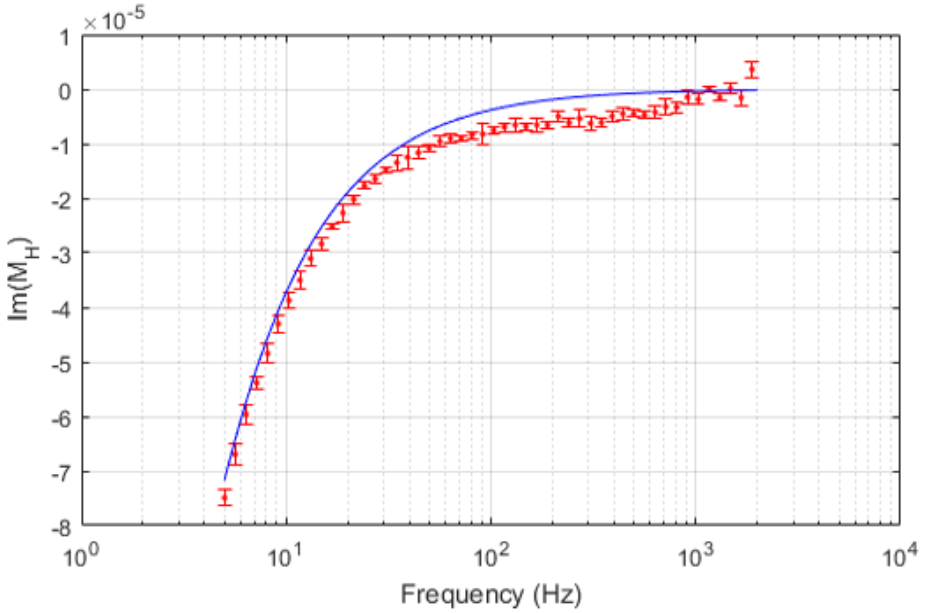

Figure 5.3. The imaginary part of the complex open-circuit voltage sensitivity measurements plotted versus frequency with NIST type A uncertainty and the simple, high-pass equivalent-circuit model for H48, serial number two, from a data set taken at 500 psi and 39.6°C

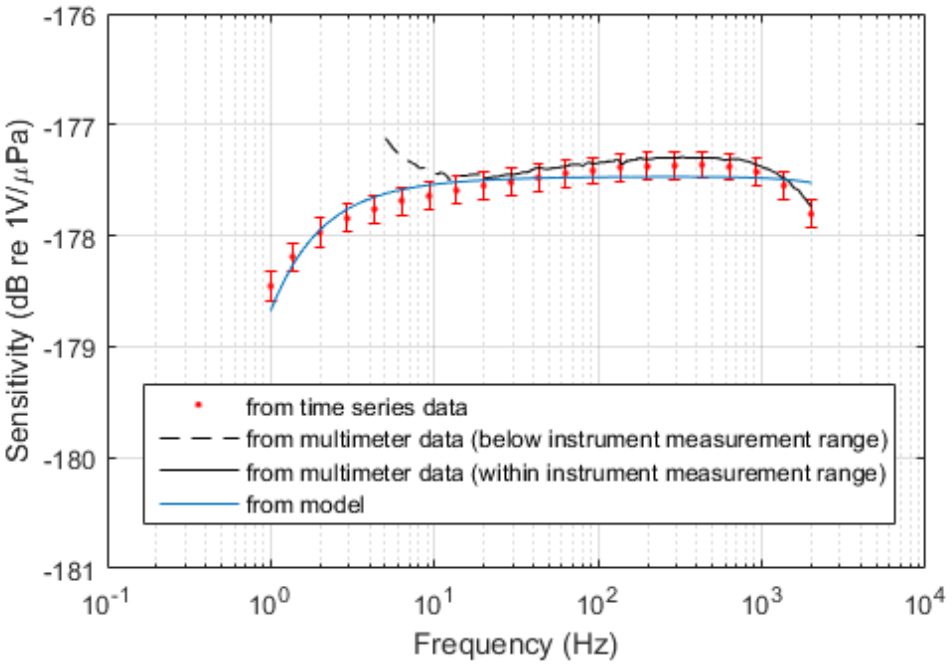

Figure 5.4. Open-circuit voltage sensitivity magnitude of H48, serial number four, comparison between times series measurements, RMS measurements, and a simple circuit model for a data set at 1000 psi and 3.2°C

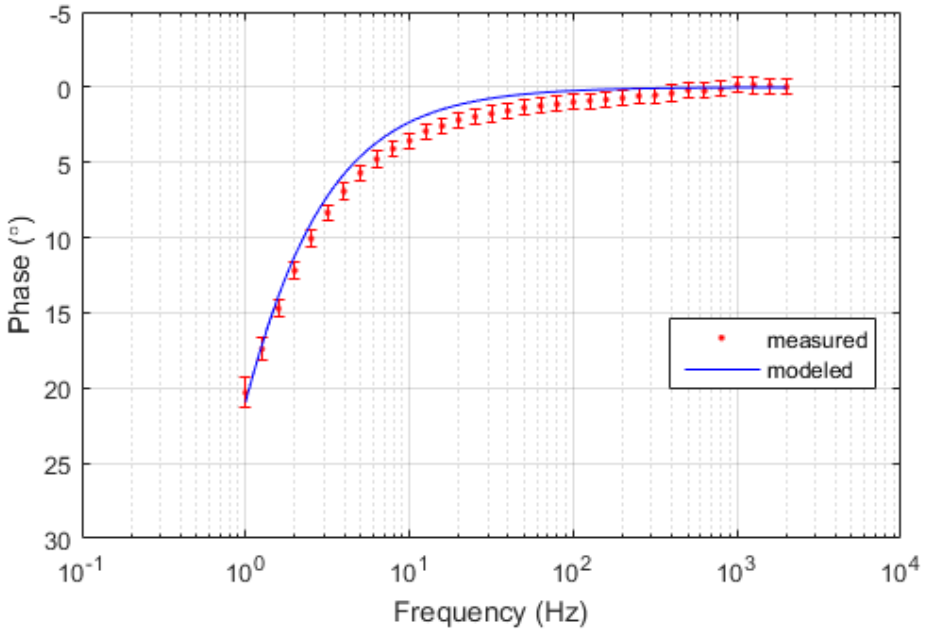

Figure 5.5. Phase response of H48, serial number four, comparison between times series measurements and a simple circuit model for a data set at 1000 psi and 3.2°C

CHAPTER 6:
Conclusion

A determination of the phase as well as the magnitude of a hydrophone's free-field voltage sensitivity was incorporated into the USRD reciprocity coupler calibration procedure by using the hydrophone sensitivity equation for a reciprocity calibration, as shown in Equation 2.6, with complex voltage inputs and a complex reciprocity parameter, given in Equation 2.17 . The complex input signals are calculated from time series measurements using a least squares estimator.

The physical setup remains the same as the previous, magnitude only, calibration setup, with data acquisition equipment added to record time series data in place of the RMS multimeters. The electronics add their own phase errors to the system, which must be separately measured and removed to isolate the phase response of the hydrophone under test.

Data sets were recorded back-to-back on H48 hydrophones using the standard RMS multimeters and new data acquisition equipment to record time series measurements. The magnitude calculated from these data sets agreed within measurement uncertainty. Both magnitude and newly incorporated phase data were fitted to a simple, RC high-pass filter equivalent circuit model of the hydrophone behavior at low frequencies. The magnitude data fit the model within measurement uncertainty across the applicable frequency range, although the hump in the higher frequencies was not predicted. The phase data fit well in the lower frequency range, of greatest interest in this report, but did not fit within measurement uncertainty in the middle of the frequency range.

Both magnitude and phase response began to roll off as frequencies approached 1 Hz from above, but the trend is easier to see in the phase data, which begins to roll off a decade higher than the magnitude data for a given cutoff frequency. The phase data were extrapolated with the equivalent-circuit model to estimate the cutoff frequency of the hydrophone — 0.3 Hz for H48 SN4 — which is greater than measured previously when the H48 was first constructed [14]. The higher cut-off frequency could lead to inaccuracies when measuring phase with an H48 hydrophone or associated secondary references under the assumption

that phase is constant down to 1 Hz.

Errors and uncertainties in the calibration are similar to that calculated previously [9] for the magnitude-only system, with new errors for the new data acquisition equipment. Additional errors and uncertainties had to be accounted for in the phase measurements, the majority of which come from the electronic equipment. Uncertainty from random error was calculated from the covariance matrix of the complex sensitivity data.

Additional acoustic sources of error come into play higher in the H48 frequency range, and should be modeled in future studies of this coupler. The irregularities in the shape of the coupler, the size of the reciprocal transducers compared to the coupler and their position within, and viscous effects can be estimated with a lumped parameter model, but would be best addressed through finite element analysis.

CHAPTER 7:
Future Work

Some features of the coupler do not conform to the simplifying assumptions of the coupler diagram in Figure 2.3 and lead to errors not treated in this report. These errors arise from the fact that the reciprocal transducers are 2.54-cm diameter spheres mounted inside the coupler walls, and the coupler itself has a shallow T-shaped branch at its center, where the hydrophone mounts. Future work should address these differences through a lumped parameter, or preferably, a finite-element model. Figure 7.1 shows a scale diagram of a cross section through the center of the coupler cavity. X and Y are the spherical elements of the reciprocal transducers and H is the hydrophone element.

The spherical transducers mounted inside the coupler walls are not necessarily stationary and do not occupy the full cross section of the coupler, leaving a small cavity between them and each end of the coupler. Incomplete cross sectional coverage leads to a radiation mass term in the acoustical transfer impedance. Space on either side of the reciprocal transducers where the flow converges and diverges contributes inertia and a Helmholtz resonance. Another divergence in the flow occurs at the T-shaped branch. These contributions can be captured by modifying the coupler compliance to be a frequency dependent, effective compliance. These effects only contribute to the acoustic radiation reactance of the coupler and therefore only affect the magnitude of the coupler calibrations, not the phase. However,

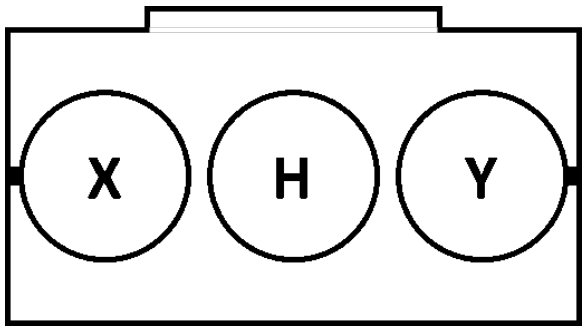

Figure 7.1. Coupler scaled diagram with reciprocal transducers X and Y, and hydrophone H

viscous effects not presently accounted for in modeling the acoustic field within the coupler could introduce phase errors.

Shortcomings in the simplified circuit model probably lead to a poor fit in the phase data in the middle of the frequency range. Adding more detail to the model of the preamplifier could help explain these discrepancies.

Also worth noting, in cases where the NIST type B error is much larger than the NIST type A error, fitting a model using an unweighted, nonlinear least-squares approach, as done in this report, will give similar results as a weighted, nonlinear least-squares fit. In cases where the NIST type A error is more significant, using a weighted fitting algorithm should improve the model results.

List of References

[1] L. D. Luker and A. L. V. Buren, "Phase calibration of hydrophones," *J. Acoust. Soc. Am.*, vol. 7, no. 2, pp. 516–519, Aug. 1981.

[2] G. Hayman, Y. Wang, and S. Robinson, "A comparison of two methods for phase response calibration of hydrophones in the frequency range 10–400 kHz," *J. Acoust. Soc. Am.*, vol. 133, no. 2, pp. 750–759, Feb. 2013.

[3] C. C. Sims and T. A. Henriquez, "Reciprocity calibration of a standard hydrophone at 16000 psi," *J. Acoust. Soc. Am.*, vol. 36, no. 9, pp. 1704–1707, Apr. 1964.

[4] R. Bobber, *Underwater Electroacoustic Measurements*. Los Altos Hills, CA: Peninsula Publishing, 1990.

[5] R. J. Bobber, "General reciprocity parameter," *J. Acoust. Soc. Am.*, vol. 39, no. 4, pp. 680–687, 1966.

[6] P. Vanicek, "Further development and properties of the spectral analysis by least-squares," *Astrophys. Space Sci.*, vol. 12, no. 1, pp. 10–33, July 1971.

[7] J. Taylor and S. Hamilton, "Some tests of the Vanicek method of spectral analysis," *Astrophys. Space Sci.*, vol. 17, no. 2, pp. 357–367, Aug. 1972.

[8] S. E. Crocker, "Measurement of acoustic insertion loss in a large nominally transparent material sample," *US Navy Journal of Underwater Acoustics*, vol. 63, JUA_2014_041_O, Mar. 2014.

[9] J. F. Zalesak, "Transfer coupler reciprocity: A new low-frequency coupler-reciprocity technique for the absolute calibration of field hydrophones under full environmental conditions," *J. Acoust. Soc. Am.*, vol. 105, no. 4, pp. 2342–2349, April 1999.

[10] *Device Specification: NI-6259. M Series Data Acquisition: 21AI, 1.25 MS/s, 48 DIO, 4 AO.*, National Instruments, Austin, TX, 2015.

[11] W. C. Young, *Roark's Forumulas for Stress and Strain*, 6th ed. New York: McGraw-Hill, 1989.

[12] S. Black and C. Siders, "Finite element modeling for the low frequency facility's reciprocity coupler," January 1995, unpublished.

[13] S. E. Crocker and R. R. Smalley, "Calibration of a digital hydrophone line array at low frequency," *IEEE J. Oceanic. Eng.*, vol. PP, no. 99, pp. 1–1, Apr. 2016, doi: 10.1109/JOE.2016.2527118.

[14] L. E. Ivey, "High-pressure piezoelectric ceramic hydrophone for infrasonic and audio frequencies USRD Type H48," Naval Research Laboratory, Tech. Rep. 7260, 1971.

[15] A. C. Tims and T. A. Henriquez, "Hydrophone phase stability analysis at frequencies below 100 Hz," Naval Research Laboratory, Tech. Rep. 8314, July 1979.

[16] *MATLAB and Optimization Toolbox Release 2015b*, The Mathworks Inc., Natick, MA, 2015.

[17] "Local calibration procedure: Hydrophones using LF reciprocity calibration," NAVSEA, Tech. Rep. LCP-17-NRA-004, July 2014.

[18] B. N. Taylor and C. E. Kuyatt, "Guidlines for evaluating and expressing the uncertainty of NIST measurement results," National Institute of Standards and Technology, Gaithersburg, MD, Tech. Rep. 1297, Sep. 1994.

[19] N. M. Ridler and M. J. Salter, "An approach to the treatment of uncertainty in complex s-parameter measurements," *Metrologia*, vol. 39, pp. 295–302, Feb. 2002.

[20] B. D. Hall, "Calculating measurement uncertainty for complex-valued quantities," *Meas. Sci. Technol.*, vol. 14, pp. 368–375, Feb. 2003.

[21] D. C. Lay, *Linear Algebra and its Applications*, 4th ed. Pearson Education, 2012.

[22] R. Timme, "Speed of sound in castor oil," *J. Acoust. Soc. Am.*, vol. 52, no. 3 (part 2), pp. 989–992, Mar. 1972.

[23] A. Sedra and K. Smith, *Microelectronic Circuits*. New York, NY: Oxford Univ. Press, 2004.

[24] J. Stallard, "Some thermodynamic properties of castor oil vs. temperature and pressure," United States Naval Ordnance Laboratory, White Oak, MD, Tech. Rep. 66-68, Apr. 1966.

Initial Distribution List

1. Defense Technical Information Center
   Ft. Belvoir, Virginia

2. Dudley Knox Library
   Naval Postgraduate School
   Monterey, California